

## **INFORMATION TO USERS**

**This manuscript has been reproduced from the microfilm master. UMI films the text directly from the original or copy submitted. Thus, some thesis and dissertation copies are in typewriter face, while others may be from any type of computer printer.**

**The quality of this reproduction is dependent upon the quality of the copy submitted. Broken or indistinct print, colored or poor quality illustrations and photographs, print bleedthrough, substandard margins, and improper alignment can adversely affect reproduction.**

**In the unlikely event that the author did not send UMI a complete manuscript and there are missing pages, these will be noted. Also, if unauthorized copyright material had to be removed, a note will indicate the deletion.**

**Oversize materials (e.g., maps, drawings, charts) are reproduced by sectioning the original, beginning at the upper left-hand corner and continuing from left to right in equal sections with small overlaps. Each original is also photographed in one exposure and is included in reduced form at the back of the book.**

**Photographs included in the original manuscript have been reproduced xerographically in this copy. Higher quality 6" x 9" black and white photographic prints are available for any photographs or illustrations appearing in this copy for an additional charge. Contact UMI directly to order.**

# **UMI**

**A Bell & Howell Information Company  
300 North Zeeb Road, Ann Arbor MI 48106-1346 USA  
313/761-4700 800/521-0600**



**University of Alberta**

**A Fatigue Crack Growth Model With  
Mean Stress Effects**

by

**Carlos Henrique de Noronha Motta**



A thesis submitted to the Faculty of Graduate Studies and Research in partial fulfillment of the requirements for the degree of **Master of Science**

**Department of Mechanical Engineering**

**Edmonton, Alberta**

**Spring 1997**



National Library  
of Canada

Acquisitions and  
Bibliographic Services

395 Wellington Street  
Ottawa ON K1A 0N4  
Canada

Bibliothèque nationale  
du Canada

Acquisitions et  
services bibliographiques

395, rue Wellington  
Ottawa ON K1A 0N4  
Canada

*Your file* *Votre référence*

*Our file* *Notre référence*

**The author has granted a non-exclusive licence allowing the National Library of Canada to reproduce, loan, distribute or sell copies of his/her thesis by any means and in any form or format, making this thesis available to interested persons.**

**The author retains ownership of the copyright in his/her thesis. Neither the thesis nor substantial extracts from it may be printed or otherwise reproduced with the author's permission.**

**L'auteur a accordé une licence non exclusive permettant à la Bibliothèque nationale du Canada de reproduire, prêter, distribuer ou vendre des copies de sa thèse de quelque manière et sous quelque forme que ce soit pour mettre des exemplaires de cette thèse à la disposition des personnes intéressées.**

**L'auteur conserve la propriété du droit d'auteur qui protège sa thèse. Ni la thèse ni des extraits substantiels de celle-ci ne doivent être imprimés ou autrement reproduits sans son autorisation.**

0-612-21163-0

**I would like to dedicate this work to my wife Claudete,  
my parents, my two brothers, and nephew.**

## **ABSTRACT**

A fatigue crack growth model with mean stress effects has been developed for low and intermediate values of the stress intensity factor range  $\Delta K$ , and Mode I loading. This model incorporates mechanical, cyclic and fatigue properties of the material as well as a material length parameter associated with a "process zone" immediately ahead of the crack tip.

A model has been proposed by Kujawski and Ellyin [1] which account for stress ratio  $R$  effects on the fatigue crack growth behaviour at low and intermediate values of the stress intensity factor range. The fatigue failure criterion adopted within the "process zone" was based on the product of stress range and plastic strain range, and the effect of the mean stress  $\sigma_m$  was taken into account through Raske & Morrow's [3] relationship. This model showed good predictions for the low and intermediate values of the stress ratio, however, it tended to underestimate the mean stress effect on the fatigue crack growth for high  $R$  ratios.

The present model was developed in order to improve the predictions of the crack growth rate values for low and intermediate stress intensities for all values of  $R$ . This was achieved by adopting a fatigue failure criterion based on the total cyclic strain energy density as a damage parameter to describe the fatigue fracture process within the "process zone".

A new equation for the calculation of the total cyclic strain energy density is introduced,

**based on the calculation of the elastic component of the total cyclic strain energy density.**

**The predictions of the proposed model were compared with experimental data, and with the results obtained by Kujawski and Ellyin's model.**

## **ACKNOWLEDGEMENT**

**I would like to express my appreciation and thanks to Dr. F. Ellyin for his supervision, and to Dr. D. Kujawski for his assistance.**



## **TABLE OF CONTENTS**

<b><u>ITEM</u></b>	<b><u>DESCRIPTION</u></b>	<b><u>PAGE</u></b>
1.0	Introduction	1
2.0	Background	4
3.0	Study of the model proposed by Kujawski and Ellyin	9
4.0	Development of a model based on the Total Cyclic Strain Energy Density as a failure criteria in the process zone	14
4.1	Monotonic stress and strain distribution ahead of the crack tip.	15
4.2	Cyclic stress and strain distribution ahead of the crack tip.	18
4.3	Total Cyclic Strain Energy Density	20
4.4	Derivation of the Fatigue Crack Growth Model	23
5.0	Comparison of the proposed crack growth model with experimental data	30
6.0	Conclusions	31
7.0	References	32

## **LIST OF TABLES**

<b><u>TABLE</u></b>	<b><u>DESCRIPTION</u></b>	<b><u>PAGE</u></b>
1	Mean Stress Values Equivalent to the Best Fit Values of $(da/dN)$ vs. $\Delta K$ for A533-B1 Steel.	37
2	Mean Stress Values Equivalent to the Best Fit Values of $(da/dN)$ vs. $\Delta K$ for 4340 Steel.	42
3	Cyclic Strain Components as a Function of $\Delta K$ for A533-B1 steel.	44
4	Cyclic Strain Components as a Function of $\Delta K$ for 4340 steel.	49
5	Maximum and Minimum Stresses within the Process Zone as a Function of $\Delta K$ for A533-B1 steel.	51
6	Maximum and Minimum Stresses within the Process Zone as a Function of $\Delta K$ for 4340 steel.	57
7	Material's Cyclic and Fatigue Properties.	58
8	Threshold Stress Intensity Factors $\Delta K_{th}$ [MPa m] as a Function of R, and process zone sizes $\delta^*$ .	59
9	Comparison of $(da/dN)$ vs. $\Delta K$ Values for A533-B1 Steel. Equation 11 (Kujawski-Ellyin), Best Fit, and the Proposed Equation 56.	60
10	Comparison of $(da/dN)$ vs. $\Delta K$ Values for 4340 Steel. Equation 11 (Kujawski-Ellyin), Best Fit, and the Proposed Equation 56.	65
11	Comparison of $(da/dN)$ vs. $\Delta K$ Values for AISI 8630 Cast Steel. Equation 11 (Kujawski-Ellyin), Best Fit, and the Proposed Equation 56.	67

12	<b>Comparison of <math>(da/dN)</math> vs. <math>\Delta K</math> Values for C-Mn Cast Steel. Equation 11 (Kujawski-Ellyin), Best Fit, and the Proposed Equation 56.</b>	69
13	<b>Comparison of <math>(da/dN)</math> vs. <math>\Delta K</math> Values for Mn-Mo Cast Steel. Equation 11 (Kujawski-Ellyin), Best Fit, and the Proposed Equation 56.</b>	71
14	<b>Comparison of <math>(da/dN)</math> vs. <math>\Delta K</math> Values for 0050A Cast Steel. Equation 11 (Kujawski-Ellyin), Best Fit, and the Proposed Equation 56.</b>	73
15	<b>Comparison of <math>(da/dN)</math> vs. <math>\Delta K</math> values for Aluminum 7075-T6. Best Fit through the experimental data points, and the proposed Equation 56.</b>	75
16	<b>Comparison of <math>(da/dN)</math> vs. <math>\Delta K</math> values for Aluminum 2024-T3. Best Fit through the experimental data points, and the proposed Equation 56.</b>	81
17	<b>Standard Deviation of the proposed model, Equation 64, and Kujawski and Ellyin's model, Equation 9, compared with the best fit (Least-Squares) through the experimental data.</b>	85

## **LIST OF FIGURES**

<b><u>FIGURE</u></b>	<b><u>DESCRIPTION</u></b>	<b><u>PAGE</u></b>
1	Schematic illustration of the mean stress $\sigma_m$ effect on the fatigue crack growth rate.	87
2	Schematic illustration of the mean stress $\sigma_m$ effect on the fatigue crack growth rate of some particular aluminum alloys.	88
3	Correlation of Schwalbe's crack growth model with the experimental results for AlZnMgCu0.5 aluminum alloy.	89
4	Correlation of Radon's crack growth model with the experimental results for BS4360-50D steel.	90
5	Schematic plot of the cyclic stress distribution within the plastic zone.	91
6	Correlation of the Kujawski-Ellyin model with the experimental data for A533-B1 steel.	92
7	Correlation of the Kujawski-Ellyin model with the experimental data for 4340 steel.	93
8	Correlation of the Kujawski-Ellyin model with the experimental data for AISI 8630 cast steel.	94
9	Correlation of the Kujawski-Ellyin model with the experimental data for C-Mn cast steel.	95
10	Correlation of the Kujawski-Ellyin model with the experimental data for Mn-Mo cast steel.	96

11	<b>Correlation of the Kujawski-Ellyin model with the experimental data for 0050A cast steel.</b>	97
12	<b>Mean stress distribution for A533-B1 steel.</b>	98
13	<b>Definition of the elastic, plastic and total cyclic strain energy density.</b>	99
14	<b>Mean stress effect in the hysteresis loop.</b>	100
15	<b>Correlation of the proposed model with the experimental data for A533-B1 steel.</b>	101
16	<b>Correlation of the proposed model with the experimental data for 4340 steel.</b>	102
17	<b>Correlation of the proposed model with the experimental data for AISI 8630 cast steel.</b>	103
18	<b>Correlation of the proposed model with the experimental data for C-Mn cast steel.</b>	104
19	<b>Correlation of the proposed model with the experimental data for Mn-Mo cast steel.</b>	105
20	<b>Correlation of the proposed model with the experimental data for 0050A cast steel.</b>	106
21	<b>Correlation of the proposed model with the experimental data for 7075-T6 aluminum.</b>	107
22	<b>Correlation of the proposed model with the experimental data for 2024-T3 aluminum.</b>	108

## **LIST OF SYMBOLS**

<b>a</b>	<b>crack length</b>
<b>b</b>	<b>fatigue strength exponent</b>
<b>c</b>	<b>fatigue ductility exponent</b>
<b>E</b>	<b>Young's Modulus</b>
<b>K</b>	<b>stress intensity factor</b>
<b><math>K_{max}</math></b>	<b>maximum stress intensity factor</b>
<b><math>\Delta K</math></b>	<b>stress intensity factor range</b>
<b><math>\Delta K_{th}</math></b>	<b>threshold stress intensity factor range</b>
<b>n</b>	<b>strain hardening exponent</b>
<b>n'</b>	<b>cyclic strain hardening exponent</b>
<b>N</b>	<b>number of cycles</b>
<b><math>N_f</math></b>	<b>number of cycles to failure</b>
<b>R</b>	<b>stress or load ratio</b>
<b><math>R_\sigma</math></b>	<b>stress ratio in the process zone</b>
<b><math>R_\sigma'</math></b>	<b>stress ratio at <math>x = r_c</math></b>
<b><math>r_c</math></b>	<b>cyclic plastic zone size</b>
<b><math>r_m</math></b>	<b>monotonic plastic zone size</b>
<b><math>\Delta W^t</math></b>	<b>total strain energy density</b>
<b><math>\Delta W^e</math></b>	<b>elastic component of the cyclic strain energy density</b>
<b><math>\Delta W^p</math></b>	<b>plastic component of the cyclic strain energy density</b>
<b>x</b>	<b>distance from the crack tip</b>
<b><math>\alpha</math></b>	<b>constant</b>

$\varepsilon$	strain
$\varepsilon_f$	true fracture strain
$\varepsilon_f'$	fatigue ductility coefficient
$\Delta\varepsilon$	total cyclic strain range
$\Delta\varepsilon^e$	elastic component of the cyclic strain range
$\Delta\varepsilon^p$	plastic component of the cyclic strain range
$\kappa$	energy coefficient
$\rho_c$	radius of the blunted crack tip
$\sigma$	stress
$\sigma_y$	stress component perpendicular to the plane of the crack
$\sigma_a$	stress amplitude within the process zone
$\sigma_f'$	fatigue strength coefficient
$\sigma_m$	mean stress within the process zone
$\sigma_{max}$	maximum stress within the process zone
$\sigma_0$	monotonic tensile yield stress
$\sigma_0'$	cyclic tensile yield stress
$\Delta\sigma$	stress range
$\delta^*$	size of the "process zone".
$\Psi$	function of $\Delta\sigma$ , $\sigma_a$ and $\sigma_m$

## 1.0 INTRODUCTION

The examination of test specimen surfaces during and after low cycle fatigue tests indicate that the major portion of the specimen life is consumed with the propagation of cracks [15]. The realization by the investigators that the low cycle fatigue damage process is predominantly crack growth, has led them to the development of several models which attempt to correlate the low cycle fatigue properties with the crack growth properties of materials.

The fatigue crack growth rate can be related to the cyclic fatigue damage process of the material at the process zone immediately ahead of the crack tip. The existence of this small plastic strain zone ahead of the crack tip can be understood based on the concepts of the continuum theory of plasticity which predicts an infinite strain concentration at the tip of a crack. Since the concept of a homogeneous continuum breaks down before this stage is reached, it seems reasonable to base the conditions for fracture, not on the local strain at the crack tip, but rather on the average strain in a small region immediately ahead of the crack, named here as the process zone [13], and located within the crack tip plastic zone.

In the early attempts to correlate the fatigue crack propagation rate with the cyclic stress-strain and fatigue properties of materials, several investigators tried to describe the behaviour of the material in the process zone through correlation with the fatigue behaviour of a smooth uniaxial specimen [4-6]. These models considered a fatigue damage zone immediately ahead of the crack tip which is modelled as a uniaxial fatigue element.

In most practical applications, a fatigue loading spectrum composed solely of fully reversed fatigue cycles does not yield a real representation of the material's expected service loading. In these cases it is necessary to include the effect of the mean stress  $\sigma_m$  in the fatigue crack growth of the material, since this will have an effect in the life of the structure or component. A positive mean stresses will cause a reduction in the fatigue life of the material, and a negative mean stress will have a reversed effect. The prediction of the mean stress effect is very important for spectrum loading where the stress ratio changes frequently, and its effect in the component life must be determined specially for the cases where crack growth retardation and/or acceleration are taken into account, in which case the designer seeks an optimum strength/weight ratio. The stress ratio and the mean stress are directly related, i.e. an increase in the stress ratio will result in an increase in the mean stress.

The effect of the mean stress on the crack growth rate are shown in Figures 1 and 2 by the  $(da/dN)$  vs.  $\Delta K$  diagram. The effect shown in Figure 1 is observed in aluminum alloys [26], carbon and low carbon steels [27,32], ferritic and perlitic steels [28,33], stainless steel [29], cast steel [30,16] and nickel alloys [31], where the effect of the mean stress



is more pronounced in the lower and upper regions of the  $(da/dN)$  vs.  $\Delta K$  diagram. For some metals and alloys [28,33,34,35] the effect of the mean stress, is reduced or non-existent in the center region of the diagram, i.e. these alloys respond to the effect of the mean stress as shown in Figure 2.

Some of the concepts adopted to take into account the effect of the mean stress in fatigue crack growth includes the crack closure approach, residual compressive stresses, and the environmental effects on the open surfaces of the crack tip under loading. However, the validity of these explanations are restricted to the specimen type, material and test conditions, since some materials tested in the vacuum exhibit no stress ratio effect in the rate of fatigue crack growth.

Correction factors based on the values of the threshold stress intensity factor,  $K_{th}$ , for the near threshold region, and correction factors based on the critical stress intensity factor,  $K_c$ , and stress ratio  $R$ , for the near critical region, have also been used in the crack growth analysis to account for the non-linearity of the log-log  $(da/dN)$  vs.  $\Delta K$  diagram near these two regions.

As the stress ratio increases in value, the threshold and critical stress intensity factors decrease as shown in Figures 1 and 2. Forman [24] modified the Paris [25] equation by introducing the factor:  $(1 - R)K_c - \Delta K$  to account the stress ratio, or mean stress, effect in the fatigue crack growth at the linear and critical regions of the log-log  $(da/dN)$  vs.  $\Delta K$  diagram.

The crack closure concept [19,39,40] is difficult to apply in practical analysis since it requires the calculation of the crack opening stress intensity factor  $K_{op}$ . There are very few expressions available in the literature for the opening stress intensity factor as a function of the stress ratio, such as the one proposed by Elber [19] for 2024-T3 Al alloy. In addition to that, recent experimental measurements of crack closure indicate that the crack opening load,  $P_{op}$ , is not a unique value, and it varies with the measurement location and the technique employed [44].

A number of investigations have been carried out on the relation of the stress ratio with the threshold value of the stress intensity factor range,  $\Delta K_{th}$ . The studies show that for many materials in air [26,28,32,33,36-38],  $\Delta K_{th}$  tends to decrease with the increasing  $R$ , however for some materials at a stress ratio ( $R > 0.5$ ) the sensitivity is less pronounced.

It is known that fatigue cracking is related to local reversed plastic yielding of the material in the vicinity of the crack tip [14]. Therefore, some investigators have attempted to describe the sigmoidal shape of the  $(\log da/dN)$  vs.  $\log \Delta K$  curve by developing models which consider a process zone immediately ahead of the crack tip, and a failure criterion within this process zone. These models incorporated mechanical, cyclic and fatigue properties of the materials, and they were derived based on a modification of Rice's [2] superposition method to extend the monotonic solution for the elastic-plastic stress and

strain fields ahead of the crack tip [9,10] to unloading, reloading and cyclic loading.

Equation 1 shows the total strain life approach to fatigue,

$$\frac{\Delta\epsilon}{2} = \frac{\sigma_f'}{E} (2N_f)^b + \epsilon_f' (2N_f)^c \quad (1)$$

where,  $\sigma_f'$  is the fatigue strength coefficient,  $b$  is the fatigue strength exponent,  $\epsilon_f'$  is the fatigue ductility coefficient,  $c$  is the fatigue ductility exponent,  $E$  is Young's Modulus, and  $N_f$  is the number of reversals to failure.

Some of the attempts made to model the mean stress effect in a crack growth equation, led to a modification of the strain-life expression, Equation 1.

The mean stress effect was introduced in Equation 1, by Raske and Morrow [3] in the form of a reduction factor of the fatigue strength coefficient of the material as shown in Equation 2,

$$\frac{\Delta\epsilon}{2} = \frac{(\sigma_f' - \sigma_m)}{E} (2N_f)^b + \epsilon_f' (2N_f)^c \quad (2)$$

Several models developed based on the above expression have provided a reasonable correlation with the experimental data for certain materials and not such a good correlation for others. Also, the models work only for a certain range, usually lower values of the stress ratio, and do not provide a good correlation for higher values of  $R$ .

The work reported here was carried out in an attempt to develop a crack growth model which would take into account the effect of the mean stress, and provide a good correlation with the experimental results for all values of the stress ratio, and for low and intermediate values of the stress intensity factor range,  $\Delta K$ . The model should also include fatigue, mechanical and cyclic properties of the material.

It should also be mentioned that this is a development of the model proposed by Kujawski & Ellyin [1], which in turn is a development of previous work by other investigators. Therefore, the following chapters will lead to a discussion on the work proposed by other investigators, a detailed assessment of the model proposed in reference [1] by Kujawski & Ellyin, and the development of the proposed model.

## 2.0 BACKGROUND

A number of crack growth equations have been developed for low and intermediate values of the stress intensity factor range,  $\Delta K$ , which incorporate fatigue, mechanical and cyclic properties of the material, and a failure criterion. Some of these models attempted to take into account the effects of the mean stress,  $\sigma_m$ , based on a modification of the strain-life expression introduced by Raske & Morrow [3], Equation 2.

Other models were developed which incorporated correction factors based on the values of the threshold stress intensity factor range,  $\Delta K_{th}$ , and the critical stress intensity factor,  $K_c$ . These factors were introduced in order to describe the non-linear shape of the  $(da/dN)$  vs.  $\Delta K$  diagram near the threshold and the critical values of the stress intensity factor range.

Schwalbe [20] studied the crack propagation properties of AlZnMgCu0.5 aluminum alloy based on the fractographic observations and macroscopic crack propagation measurements of the specimens under monotonic and cyclic loading. Under systematic arrangement of the results, and comparison of the data obtained for monotonic and cyclic loading, he concluded that crack propagation under both loading conditions may be governed by essentially the same micromechanisms, and may be described by the same laws of fracture mechanics.

The crack growth equation obtained by Schwalbe, for a plane strain condition, is given by Equation 3.

$$\frac{da}{dN} = \frac{(1-2\nu)^2}{(1+n)4\pi\sigma_0^2} \left[ \frac{2\sigma_0}{E\epsilon_f} \right]^{1+n} (\Delta K - \Delta K_{th})^2 \frac{K_c}{K_c - K_{max}} \quad (3)$$

where:  $\epsilon_f$  is the material's true fracture strain,  $E$  is Young's Modulus,  $n$  is the monotonic strain hardening exponent,  $\sigma_0$  is the material's monotonic tensile yield strength,  $\nu$  is Poisson's ratio, and  $K_c$  and  $K_{max}$  are the critical and the maximum values of the stress intensity factor.

It is to be noted that this equation incorporates not only the mechanical and fatigue properties of the material, but the monotonic properties as well. Note also that, the correction factor  $[K_c / (K_c - K_{max})]$  is introduced to predict the values of  $(da/dN)$  at the region near the critical value of the stress intensity factor  $K_c$ . The mean stress effect is introduced in the values of  $K_{max}$  and  $\Delta K_{th}$  since,  $K_{max} = \Delta K / (1 - R)$ , and  $\Delta K_{th}$  may be empirically determined, as proposed by Klesnil and Lukas [21]. The authors proposed the following expression for the threshold stress intensity factor range,  $\Delta K_{th} = \Delta K_{th0} (1 - R)^\mu$ , where  $\mu$  is a parameter which is chosen to fit the experimental data, and  $\Delta K_{th0}$  is the

threshold stress intensity factor range value for  $R = 0$ .

The correlation of Schwalbe's equation with the experimental results is shown in Figure 3 for AlZnMgCu0.5 aluminum alloy for  $R = 0$ .

Radon [22] proposed a crack growth model for the near threshold region which incorporated mechanical, cyclic and fatigue properties of the material, and a plastic strain,  $\Delta\epsilon^p$ , based failure criterion. He also introduced an effective stress intensity factor range,  $\Delta K_{eff}$ , which characterize the crack tip opening displacement and the strains immediately ahead of the crack tip.

Radon assumed that the crack would advance cycle by cycle by an average increment,  $\Delta a$ , into any material elements immediately ahead of the crack tip where the cyclic plastic strain range  $\Delta\epsilon^p$  reaches or exceeds the true fracture strain  $\epsilon_f$  during the loading part of the cycle, where the effective stress intensity range  $\Delta K_{eff}$  is increasing from  $K_{min,eff}$  to  $K_{max}$ .

The cyclic plastic strain range  $\Delta\epsilon^p$  at the crack front is given by the expression,

$$\Delta\epsilon^p = \frac{2\sigma_0'}{E} \left[ \frac{\Delta K^2}{4(1+n')\pi\sigma_0'^2 x} \right]^{\frac{1}{1+n'}} \quad (4)$$

where:  $\sigma_0'$  is the cyclic yield stress,  $n'$  is the cyclic strain hardening exponent,  $x$  is the distance from the crack tip, and to eliminate the singularity at ( $x = 0$ ) we introduce the crack tip blunting radius  $\rho_c$ , which is associated with the threshold stress intensity factor, and replace  $x$  with  $x + \rho_c$  in Equation 4.

Over the distance  $\Delta a$ , the strains are equal to or greater than the material's true fracture strain  $\epsilon_f$ , therefore the average crack increase per cycle is given by substituting  $\Delta a$  for  $x$  in Equation 4 and equating it to  $\epsilon_f$ . Therefore, solving for  $\Delta a$  which is the average crack growth per cycle or ( $da/dN$ ), Radon obtained the following expression for the crack growth equation, for a plane strain condition,

$$\frac{da}{dN} = \frac{2^{1+n'}(1-2\nu)^2(\Delta K_{eff}^2 - \Delta K_{th,eff}^2)}{4(1+n')\pi\sigma_0^{1+n'}E^{1+n'}\epsilon_f^{1+n'}} \quad (5)$$

where:  $\Delta K_{th,eff}$  is the effective threshold stress intensity factor range, and it is associated

with a maximum critical value of the crack tip blunting radius,  $\rho_c$ , in connection with a non-propagating crack.

The correlation of Radon's equation with the experimental data for BS4360-50D steel is shown in Figure 4.

Kujawski & Ellyin [1] proposed a fatigue crack growth model with the load ratio effect which incorporates the bulk cyclic and low cycle fatigue properties of the material. The authors defined a process zone,  $\delta^*$ , immediately ahead of the crack tip where, due to non-proportional plasticity and crack tip blunting, the stress and strain have a finite magnitude with a small gradient.

A failure criterion based on the product of the stress range,  $\Delta\sigma$ , and the plastic strain range,  $\Delta\varepsilon^p$ , was adopted within the process zone. The product of the stress and plastic strain range is proportional to the plastic strain energy density dissipated by the fractured material elements within the process zone. The elastic strain energy was not taken into consideration since within the process zone the plastic strain is much greater than the elastic strain  $\Delta\varepsilon^p \gg \Delta\varepsilon^e$ .

Kujawski and Ellyin defined three regions ahead of a growing crack as shown in Figure 5. Region I is the cyclic plastic zone  $r_c$ , where plastic deformation takes place during the loading and unloading half-cycles. Region II, between the monotonic plastic zone,  $r_m$ , and the cyclic plastic zone,  $r_c$ , where plastic deformation occurs only during the loading part of the half-cycle, and it is elastic during the unloading part. Region III is the elastic zone beyond the monotonic plastic zone,  $r_m$ , where cyclic strains are fully elastic during the loading and unloading.

Contrary to the case of a smooth uniaxial specimen, the stress ratio within the plastic zone is not constant. The distribution of the stress and strain within the plastic zone is highly inhomogeneous. The maximum stress distribution is the same as for the monotonic loading case, as given for Mode I cracking by McClintock [13] from a modification of Rice's [2] solution for the stresses and strains within the plastic zone for the tearing mode, Mode III cracking. The maximum stress is given by the following expression,

$$\sigma_{\max} = \sigma_0' \left[ \frac{K_{\max}^2}{(1+n') \pi \sigma_0'^2 x} \right]^{\frac{n'}{1+n'}} \quad (6)$$

where:  $x$  is the distance from the crack tip, and the other symbols have been previously defined.

The minimum stress within the plastic zone is obtained by applying Rice's [2] superposition argument of the reverse flow during unloading, and it is shown by the dashed line in Figure 5. The stress ratio within the plastic zone can now be calculated from:  $R_\sigma = \sigma_{\min} / \sigma_{\max}$ , where  $\sigma_{\min}$  is given by:  $\sigma_{\min} = \sigma_{\max} - \Delta\sigma$ , and the stress range is given from a modification of Rice's monotonic solution by,

$$\Delta\sigma = 2\sigma'_0 \left[ \frac{\Delta K^2}{4(1+n')\pi\sigma'_0{}^2 x} \right]^{\frac{n'}{1+n'}} \quad (7)$$

Within the process zone  $\delta^*$ , the maximum stress and the stress range are calculated from Equations 6 and 7 by replacing  $x$  with  $\delta^*$ .

The mean stress effect was taken into account based on Morrow's [23] modification of the stress-life expression and is given by the expression,

$$\frac{\Delta\sigma}{2} = (\sigma'_f - \sigma_m) (2N_f)^b \quad (8)$$

The effect of the mean stress is thus equivalent to a reduction of the fatigue strength coefficient. A negative mean stress would have a reversed effect.

Therefore, with the definition of the stress ratio,  $R_\sigma$ , in the plastic zone, and the failure criterion based on the product of the stress range and the plastic strain range, Kujawski and Ellyin obtained the following crack growth equation,

$$\frac{da}{dN} = 2\delta^* \left[ \frac{\Delta K^2 - \Delta K_m^2}{4(1+n')\pi E (\sigma'_f - \sigma_m) \epsilon'_f \delta^*} \right]^{-\frac{1}{b+c}} \quad (9)$$

where:  $b$  is the fatigue strength exponent,  $c$  is the fatigue ductility exponent,  $\delta^*$  defines the process zone size which is a material length parameter,  $\Delta K_m$  is the threshold stress intensity factor range, and  $\sigma_m$  is the mean stress value within the process zone which is given by the relation,

$$\sigma_m = \frac{1+R_\sigma}{2} \sigma_{max} \quad (10)$$

in which,  $\sigma_{max}$  is the maximum stress within the process zone, and it is given by Equation 6 with the variable  $x$  replaced with  $\delta^*$ .

The correlation of Kujawski and Ellyin's model with the experimental data is shown in Figures 6 to 11 for A533-B1 steel, 4340 steel, AISI 8630 cast steel, C-Mn cast steel, Mn-Mo cast steel, and SAE 0050A cast steel, respectively.

It can be noticed the tendency of Equation 9 to underestimate the values of  $(da/dN)$  in the near threshold region for higher values of the stress ratio,  $R$ , and lower values of the stress intensity factor range,  $\Delta K$ .

The analysis to follow is developed based on Kujawski and Ellyin's assumptions for the cyclic stress and strain distribution in the plastic zone ahead of the crack tip. However, the effect of the mean stress is taken into account in a different manner, by assuming a new failure criterion within the process zone.

### **3.0 STUDY OF THE MODEL PROPOSED BY KUJAWSKI AND ELLYIN**

A study was carried out in an attempt to identify under what conditions the model proposed by Kujawski and Ellyin [1] would tend to underestimate the crack growth rate values ( $da/dN$ ) for high values of the stress ratio,  $R$ . The results of this study are reported in this section.

A brief description of the model was given in the previous section. The key parameter of the model is the definition of the stress ratio within the plastic zone,  $R_p$ , since the mean stress value is derived directly from this variable. Within the plastic zone the stress ratio is not constant as shown by the maximum and minimum stress distribution plots in Figure 5. The value of  $R_p$  is defined within the plastic zone based on Rice's [2] solution for the stress distribution within the plastic zone, as modified by McClintock [13] for Mode I cracking. These equations were then modified for the cyclic loading, since Rice's solution is for monotonic loading.

Basically, Kujawski and Ellyin [1] identified three different physical phases of the plastic zone ahead of a stable growing crack due to the local elastic-plastic material behaviour as shown in Figure 5. The process zone, denoted by  $\delta^*$ , immediately ahead of the crack tip, whereby due to the crack tip blunting and non-proportional plasticity, the stresses and strains have a finite magnitude with a small gradient. The reversed, or cyclic, plastic zone,  $r_c$ , where plastic deformation takes place during the loading and unloading half-cycles, and the monotonic plastic zone,  $r_m$ . In between the monotonic plastic zone and the cyclic plastic zone, plastic deformation takes place only during the loading part of the cycle and is elastic during the unloading part. The region beyond the monotonic plastic zone, is the elastic zone, where cyclic strains are fully elastic during loading and unloading.

The failure criterion adopted by the authors was based on the product of stress range and plastic strain range ( $\Delta\sigma\Delta\varepsilon^p$ ), which is proportional to the absorbed plastic strain energy density. The effects of the elastic strain component, which is associated with the elastic strain energy, were not taken into account, since within the process zone the plastic strain energy is much greater than the elastic one, i.e.  $\Delta W^p \gg \Delta W^e$ . The effect of the mean stress  $\sigma_m$  was taken into account according to Raske and Morrow's [3] modification of the strain-life expression, Equation 2, to account for mean stress effects.

It was mentioned earlier that the expression obtained by Kujawski and Ellyin [1] for the fatigue crack growth equation had the form as shown by Equation 9, and repeated below,



$$\frac{da}{dN} = 2\delta^* \left[ \frac{\Delta K^2 - \Delta K_{th}^2}{4(1+n')(\sigma_f' - \sigma_m)\epsilon_f' \pi E \delta^*} \right]^{-\frac{1}{b+c}} \quad (9)$$

The correlation of Equation 9 above with the experimental data is shown in Figures 6 to 11 for A533-B1 steel, 4340 steel, AISI 8630 cast steel, C-Mn cast steel, Mn-Mo cast steel, and SAE 0050A cast steel respectively.

The value of the mean stress,  $\sigma_m$ , within the process zone, in Equation 9, is calculated from the expression,

$$\sigma_m = \frac{\sigma_{max} + \sigma_{min}}{2} \quad (11)$$

or,

$$\sigma_m = \frac{\sigma_{max} + R_\sigma \sigma_{max}}{2} = \frac{1 + R_\sigma}{2} \sigma_{max} \quad (12)$$

where,  $\sigma_{max}$  and  $R_\sigma$  are the maximum stress and the stress ratio in the process zone.

The spread and shape of the (da/dN vs.  $\Delta K$ ) curves as a function of the stress ratio  $R_\sigma$  is then determined based on the values of  $\delta^*$ ,  $r_c$  and  $r_m$  as follows :

for  $\delta^* > r_m$  :

$$R_\sigma = R \quad (13)$$

for  $r_c \leq \delta^* \leq r_m$  :

$$R_\sigma = R_\sigma^* + \frac{\log \delta^* - \log r_c}{\log r_m - \log r_c} (R - R_\sigma^*) \quad (14)$$

for  $\delta^* < r_c$  :

$$R_\sigma = R_\sigma^* - \left( \frac{r_c - \delta^*}{r_c} \right) (1 + R_\sigma^*) \quad (15)$$

where :

$$R_\sigma^* = 1 - 2 \left[ \frac{(1-R)^2}{4} \right]^{\frac{n'}{(1+n')}} \quad (16)$$

The value of  $\sigma_{\max}$  according to Kujawski and Ellyin's model is calculated by the following expression,

$$\sigma_{\max} = \sigma_0' \left[ \frac{K_{\max}^2}{(1+n') \pi \sigma_0'^2 \delta^*} \right]^{\frac{n'}{(1+n')}} \quad (17)$$

From Figures 6 to 11 it can be seen that the upper part of the curves calculated by Equation 9, for values of  $\Delta K$  much greater than  $\Delta K_m$ , actually produces a good fit with the experimental data points. The problem is more accentuated for lower values of  $\Delta K$  at the near threshold stress intensity factor range,  $\Delta K_m$ . This indicates that the values obtained for the mean stress,  $\sigma_m$ , from Equation 12 should be higher for lower values of  $\Delta K$  in order to give higher values of  $(da/dN)$ .

In order to identify the reason for Kujawski and Ellyin's model to underestimate the values of  $(da/dN)$  for high values of  $R$ , a verification of the values calculated for the mean stress within the process zone, Equation 12, and the failure criterion adopted, was carried out.

The calculated values for the mean stress were compared with the values determined from the best fit through the experimental data points for each value of the stress ratio  $R$ , i.e. the best fit values of  $(da/dN)$  and  $\Delta K$  where applied to Equation 11, and from a reverse calculation the values of the mean stress were determined for the best fit curves for all values of  $R$ . It should be noted that the values of  $\delta^*$  used in this reverse analysis were the same ones calculated by Kujawski and Ellyin in [1].

Tables 1 and 2 show the results of this verification for A533-B1 and 4340 steels respectively. The results for A533-B1 steel are plotted in Figure 12. These tables show

the best fit values of  $(da/dN)$  and  $\sigma_m$  from the best fit through the experimental data points, and the ones calculated by Equation 12 respectively.

Figure 12 shows that the values of  $\sigma_m$  calculated from the best fit curve are higher for lower values of  $\Delta K$ , and there is a wide difference between the values calculated with Equation 12 and the best fit values. For higher values of  $\Delta K$  the difference between the best fit and the calculated values of  $\sigma_m$  decreases considerably.

Although the expression for the mean stress, Equation 12, have not provided adequate values of  $(da/dN)$  for low values of  $\Delta K$  and high values of  $R$ , the gradient of the  $\sigma_m$  values from Equation 12 does agree with the distribution of the  $\sigma_m$  values obtained from the reverse calculation based on the best fit through the experimental data points. This equation has also shown to provide adequate mean stress values for higher values of  $\Delta K$ , as shown Figures 6 to 11 from the good fit through the experimental data points for higher  $\Delta K$  values.

Based on the these observations, an investigation of the failure criterion adopted by Kujawski & Ellyin was carried out in order to identify the effects of neglecting the contribution of the elastic strain energy in the failure criteria within the process zone.

The authors in the derivation of the model described by Equation 9 adopted a failure criterion, within the process zone, based on the product of stress range  $\Delta\sigma$  and the plastic component  $\Delta\varepsilon^p$  of the total strain range ( $\Delta\varepsilon = \Delta\varepsilon^e + \Delta\varepsilon^p$ ). Therefore, they neglected the contribution of the elastic deformation which is associated with the elastic strain energy. The basis for that is, theoretically, the elastic strain is fully recoverable upon unloading of the material and it does not cause any perceivable damage when considering the specimen as a whole, i.e. its macroscopic behavior.

Perhaps at the macroscopic level, and using equations which only consider the material's macroscopic characteristics, it is adequate to ignore the damage contribution produced by the elastic strain energy. However, the authors' model is directly related to their assumption of the stress and strain distribution within the process zone, and that at the microscopic level, stresses and strains considered elastic at the macroscopic level, will produce damage at sites of strain localization in the form of thin lamellae of persistent slip bands, PSB's. This is discussed in Section 4.3.

Tables 3 and 4 show the values of the cyclic elastic strain range  $\Delta\varepsilon^e$ , the cyclic plastic strain range  $\Delta\varepsilon^p$  and the total cyclic strain range ( $\Delta\varepsilon = \Delta\varepsilon^e + \Delta\varepsilon^p$ ) calculated within the process zone as a function of  $\Delta K$  for A533-B1 and 4340 steels, respectively. The values on these two tables are for the range of experimental data available for each value of  $R$ .

The expression for the total cyclic strain range,  $\Delta\varepsilon$ , within the process zone is as follows,

$$\Delta\epsilon = \frac{2\sigma'_0}{E} \left[ \frac{\Delta K^2}{4(1+n')\pi\sigma_0'^2\delta^*} \right]^{\frac{n'}{1+n'}} + \frac{2\sigma'_0}{E} \left[ \frac{\Delta K^2}{4(1+n')\pi\sigma_0'^2\delta^*} \right]^{\frac{1}{1+n'}} \quad (18)$$

It can be noticed from Tables 3 and 4 that for low values of  $\Delta K$ , and high values of  $R$ , the cyclic elastic strain makes up a significant portion of the total cyclic strain.

#### **4.0 DEVELOPMENT OF A MODEL BASED ON THE TOTAL CYCLIC STRAIN ENERGY DENSITY AS A FAILURE CRITERION IN THE PROCESS ZONE**

Although the objective of this work was to obtain an improved crack growth equation, the basic assumptions for the distribution of the cyclic stresses and strains within the plastic zone for the model proposed by Kujawski and Ellyin [1] have been maintained. It is assumed that Equation 9 underestimates the  $(da/dN)$  values for low values of  $\Delta K$  and high values of  $R$  because of the failure criterion adopted by the authors, rather than an incorrect assumption for the distribution of the cyclic stresses and strains within the process zone.

It was previously mentioned that Kujawski and Ellyin's failure criterion, which ignored the damage contribution of the cyclic elastic strain, is a reasonable assumption for high values of the stress intensity factor range,  $\Delta K$ , and lower values of  $R$ . However, at low values of  $\Delta K$ , and high  $R$  values, the elastic strain component, which is associated with the elastic strain energy, cannot be ignored and must be included in the failure criterion. This is confirmed by inspecting tables 3 and 4, as discussed in the previous section.

#### 4.1 MONOTONIC STRESS AND STRAIN DISTRIBUTION AHEAD OF THE CRACK TIP

The uniaxial stress-strain relation for a strain-hardening material, as proposed by Ramberg-Osgood is given by,

$$\frac{\epsilon}{\epsilon_0} = \left(\frac{\sigma}{\sigma_0}\right) + \alpha \left(\frac{\sigma}{\sigma_0}\right)^{\frac{1}{n}} \quad (19)$$

where  $\sigma_0$  is the yield stress,  $\epsilon_0 = \sigma_0/E$ ,  $E$  is the Young's modulus, and  $\alpha$  and  $n$  are parameters determined from best fit of experimental data.

The applicability of Equation 19 is limited to monotonically increasing stress, or according to the plasticity theory, under the condition of no unloading.

It is generally assumed that plastic deformation is independent of the hydrostatic component of the stress,  $\sigma_{kk}$ , and is completely determined by the first invariant of the stress deviator as given by,

$$s_{ij} = \sigma_{ij} - \frac{1}{3} \sigma_{kk} \delta_{ij} \quad (20)$$

Introducing the invariant in the form of the effective stress,  $\sigma_e$ , we have,

$$\sigma_e^2 = \frac{3}{2} s_{ij} s_{ij} \quad (21)$$

The generalized stress-strain relation which reduces to Equation 8 in simple tension according to Hutchinson [9] is,

$$\frac{\epsilon_{ij}}{\epsilon_0} = \frac{1+\nu}{\sigma_0} s_{ij} + \frac{1-2\nu}{3\sigma_0} \sigma_{kk} \delta_{ij} + \frac{3}{2} \alpha \left(\frac{\sigma_e}{\sigma_0}\right)^{\frac{(1-n)}{n}} \frac{s_{ij}}{\sigma_0} \quad (22)$$

The monotonic solution for the elastic-plastic strain and stress fields ahead of the crack tip as formulated by Hutchinson [9], and Rice and Rosengren [10] are given by the

following expressions,

$$\begin{aligned}\epsilon_{ij} &= \frac{\sigma_0}{E} \left[ \left( \frac{EJ}{\alpha \sigma_0^2 I_n r} \right)^{\frac{n}{n+1}} e_{ij}^*(n, \theta) + \alpha \left( \frac{EJ}{\alpha \sigma_0^2 I_n r} \right)^{\frac{1}{n+1}} \epsilon_{ij}^*(n, \theta) \right], \\ \sigma_{ij} &= \sigma_0 \left( \frac{EJ}{\alpha \sigma_0^2 I_n r} \right)^{\frac{n}{n+1}} \sigma_{ij}^*(n, \theta)\end{aligned}\quad (23)$$

where:  $r$  and  $\theta$  are polar coordinates;  $\sigma_{ij}^*$ ,  $\epsilon_{ij}^*$  and  $e_{ij}^*$  are known dimensionless functions of the strain hardening exponent  $n$ , and  $\theta$ ; the parameter  $I_n$  is a function of  $n$  only and  $J$  is Rice's path independent integral.

The stress and strain components normal to the plane of the crack ( $\theta = 0$ ), in a plane stress condition, can be determined from Equation 23 as follows,

$$\begin{aligned}\epsilon(x, 0) &= \frac{\sigma_0}{E} \left( \frac{EJ}{\alpha I_n \sigma_0^2 x} \right)^{\frac{n}{n+1}} (\sigma_\theta^* - \nu \sigma_r^*) + \frac{\alpha \sigma_0}{E} \left( \frac{EJ}{\alpha I_n \sigma_0^2 x} \right)^{\frac{1}{n+1}} \left( \sigma_\theta^* - \frac{1}{2} \sigma_r^* \right), \\ \sigma(x, 0) &= \sigma_0 \left( \frac{EJ}{\alpha I_n \sigma_0^2 x} \right)^{\frac{n}{n+1}} (\sigma_\theta^*)\end{aligned}\quad (24)$$

where:  $\sigma_r^*$ ,  $\sigma_\theta^*$  and  $I_n$  are functions of  $n$  only and they are evaluated numerically.

Closed form solutions for the stresses and strains in the plastic zone have not yet been obtained for strain hardening materials for the opening mode, Mode I. However, Rice's [11] solution for the anti-plane shear mode, Mode III, was modified by Kujawski and Ellyin [12] in order to obtain the stresses and strains within the plastic zone. This method was developed for a Ramberg-Osgood material and it was based on an interpretation of the strain hardening exponent  $n$ .

The expressions obtained by Kujawski and Ellyin [12] for the stress and strain components normal to the crack plane ( $\theta = 0$ ) are as follows,

$$\begin{aligned}\epsilon(x, 0) &= \frac{\sigma_0}{E} \left[ \frac{K^2}{(1+n^*) \pi \sigma_0^2 x} \right]^{\frac{n^*}{n^*+1}} + \frac{\sigma_0}{E} \left[ \frac{K^2}{(1+n^*) \pi \sigma_0^2 x} \right]^{\frac{1}{n^*+1}}, \\ \sigma(x, 0) &= \sigma_0 \left[ \frac{K^2}{(1+n^*) \pi \sigma_0^2 x} \right]^{\frac{n^*}{n^*+1}}\end{aligned}\quad (25)$$

where,  $n^*$  is given by the expression,

$$n^* = \frac{W(\sigma)}{W(\epsilon)} = \frac{W^e + nW^p}{W^e + W^p} = \frac{1+n(W^p/W^e)}{1+(W^p/W^e)} \quad (26)$$

In Equation 26 when  $W^p \gg W^e$  then  $n^* = n$ , and when  $W^p \ll W^e$  then  $n^* = 1$ .  $W^e$  and  $W^p$  are the elastic and plastic components of the strain energy density and are given by the following expressions,

$$\begin{aligned}W^e &= \int_0^\epsilon E \epsilon' d\epsilon' = \frac{\sigma^2}{2E}, \\ W^p &= \int_0^{\epsilon^p} \sigma d\epsilon^p = \frac{1}{1+n} \sigma \epsilon^p\end{aligned}\quad (27)$$



## 4.2 CYCLIC STRESS AND STRAIN DISTRIBUTION AHEAD OF THE CRACK TIP

For a material subjected to cyclic loading, or deformation, the uniaxial cyclic stress-strain relationship is given by,

$$\frac{\Delta \epsilon}{2} = \frac{\Delta \epsilon^e}{2} + \frac{\Delta \epsilon^p}{2} \quad \therefore \quad \frac{\Delta \epsilon}{2} = \frac{\Delta \sigma}{2E} + \left( \frac{\Delta \sigma}{2K'} \right)^{\frac{1}{n'}} \quad (28)$$

where:  $\Delta \epsilon$  is the cyclic strain range,  $\Delta \sigma$  is the stress range,  $K'$  is the cyclic strength coefficient, and  $n'$  is the cyclic strain hardening exponent.

The expressions for the stress and strain fields ahead of the crack tip, Equations 24 and 25, are for monotonic loading. To extend the response to unloading, reloading and cyclic loading, we may use Rice's [2] plastic superposition method, which is based on the fundamental assumption that the plastic strain components at each point within the plastic zone remain proportional to each other.

Rice considered a stationary crack loaded in anti-plane shear, Mode III, under small-scale yielding. McClintock [13] discussed the analogy between Mode III and Mode I for the case where displacements parallel to the crack are small compared with those normal to the crack surface.

Therefore, Equations 24 and 25 can be modified for cyclic loading, and the cyclic stress and strain components normal to the crack plane for a plane stress condition, as given by Equation 25 become,

$$\frac{\Delta \epsilon}{2} = \frac{\sigma_0'}{E} \left[ \frac{\Delta K^2}{4(1+n')\pi\sigma_0'^2 x} \right]^{\frac{n'}{n'+1}} + \frac{\sigma_0'}{E} \left[ \frac{\Delta K^2}{4(1+n')\pi\sigma_0'^2 x} \right]^{\frac{1}{n'+1}}, \quad (29)$$

$$\frac{\Delta \sigma}{2} = \sigma_0' \left[ \frac{\Delta K^2}{4(1+n')\pi\sigma_0'^2 x} \right]^{\frac{n'}{n'+1}}$$

where,  $n'$  is given by the following expression,

$$n^{*'} = \frac{1+n' \left( \frac{\Delta W^p}{\Delta W^e} \right)}{1 + \left( \frac{\Delta W^p}{\Delta W^e} \right)} \quad (30)$$

where,  $\sigma'_0$  is the cyclic yield stress,  $\Delta\sigma$  is the stress range,  $\Delta\varepsilon$  is the strain range, and  $\Delta K$  is the stress intensity range.

The cyclic components of the elastic and plastic strain energy density for materials which follow a Masing type behaviour, for  $R \leq 0$ , are given by the expressions,

$$\Delta W^e = \frac{1}{2E} \left( \frac{\Delta\sigma}{2} + \sigma_m \right)^2 = \frac{\Delta\sigma^2}{8E} \left( 1 + \frac{\sigma_m}{\sigma_a} \right)^2 = \frac{\sigma_{max}^2}{2E} \quad , \quad (31)$$

$$\Delta W^p = \frac{1-n'}{1+n'} \Delta\sigma \Delta\varepsilon^p$$

Within the process zone  $\delta^*$ , the plastic strain range is much larger than the elastic strain range, i.e.  $\Delta\varepsilon^p \gg \Delta\varepsilon^e$ , and consequently  $\Delta W^p \gg \Delta W^e$ . With this condition we will have  $n^{*'} = n'$  in Equations 29 which can be written as,

$$\frac{\Delta\varepsilon}{2} = \frac{\sigma'_0}{E} \left[ \frac{\Delta K^2}{4(1+n')\pi\sigma_0'^2 x} \right]^{\frac{n'}{n'+1}} + \frac{\sigma'_0}{E} \left[ \frac{\Delta K^2}{4(1+n')\pi\sigma_0'^2 x} \right]^{\frac{1}{n'+1}} \quad , \quad (32)$$

$$\frac{\Delta\sigma}{2} = \sigma'_0 \left[ \frac{\Delta K^2}{4(1+n')\pi\sigma_0'^2 x} \right]^{\frac{n'}{n'+1}}$$

### 4.3 TOTAL CYCLIC STRAIN ENERGY DENSITY

The total cyclic strain energy density range,  $\Delta W^t$ , includes both the tensile elastic,  $\Delta W^{e+}$ , and plastic,  $\Delta W^p$ , components of the cyclic strain energy, shown in Figure 13, as follows,

$$\Delta W^t = \Delta W^{e+} + \Delta W^p \quad (33)$$

For materials which follow a Masing behaviour the expressions for the tensile elastic, and plastic components of the total cyclic strain energy, for  $R \leq 0$ , are as follows [14],

$$\Delta W^{e+} = \frac{1}{2E} \left( \frac{\Delta \sigma}{2} + \sigma_m \right)^2 = \frac{\Delta \sigma^2}{8E} \left( 1 + \frac{\sigma_m}{\sigma_a} \right)^2 = \frac{\sigma_{max}^2}{2E} \quad , \quad (34)$$

$$\Delta W^p = \frac{1-n'}{1+n'} \Delta \sigma \Delta \epsilon^p$$

Therefore, the expression for the total cyclic strain energy density is given as,

$$\Delta W^t = \frac{1-n'}{1+n'} \Delta \sigma \Delta \epsilon^p + \frac{1}{2E} \left( \frac{\Delta \sigma}{2} + \sigma_m \right)^2 \quad (35)$$

The tensile elastic strain energy density,  $\Delta W^{e+}$ , is associated with the tensile elastic stress and strain. The elastic strain is fully recoverable upon unloading of the specimen, and theoretically, considering the specimen as a whole, it does not cause any perceivable damage. However, it is known that cracks may initiate from essentially flaw-free regions from a macroscopic point of view, or from existing material defects such as inclusions or voids. This variation in the initiation process is one of the factors leading to the broad scatter of fatigue (S-N) data for a specific material tested at a specific stress level and load ratio  $R$ . In the case of the flaw-free regions, cracks generally initiate at the surface of the specimen from notch-like discontinuities resulting from the slip along the crystallographic planes [14].

Cyclic deformations induce microstructural changes in the bulk of the material eventually leading to some form of strain localization. These strain localization are formed at a critical stress or strain in the form of thin lamellae of persistent slip bands (PSB's). The subsequent deformation is mainly concentrated in these slip bands, and during stable cyclic response of the material the number of PSB's increase provided the applied strain

is high enough [14]. For macroscopically isotropic materials, the persistent slip bands PSB's, are major nucleation sites for cracks at the micro-notches near the surface of the specimen. Crack initiation at sites where the PSB's impinge on the grain boundaries have also been observed, leading to intercrystalline crack initiation. Intergranular and transgranular surface crack initiation sites are induced by PSB's [14].

The effect of the strain concentration mechanism just described can be observed in typical S-N type diagram, where the large scatter of fatigue data for each specific material occurs not only at the region of high stress levels, but also at the fatigue limit region, where the stresses are low. This indicates that even at low stress levels cracks initiate faster in some specimens. Although one could assume that for the specimens with shorter fatigue lives cracks were always initiated due to the presence of inclusions or voids, this would be unconservative since several, if not all, specimens of a specific material, tested at a certain load ratio  $R$ , are cut from the same material sample.

For the macroscopically isotropic material tested at stresses around its fatigue limit stress, the strains are predominantly elastic throughout the specimen. However, at the grain level of the material, at grain boundaries and at the intersection with the PSB's, the strains are plastic and they cannot be measured with the current measurement techniques, such as strain gaging.

Therefore, the elastic strain energy density term, Equation 34, being used in the failure criterion, might be interpreted as an attempt to measure, and take into consideration the plastic strain energy associated with these microscopic plastic strains which occur at grain the level.

One should notice that the expression for the elastic component of the total cyclic strain energy density  $\Delta W^e$ , which is given by the first of equations 31, can be used only for values of the stress ratio in the range  $R \leq 0$ , i.e.  $\sigma_{min} \leq 0$ . Otherwise, as shown in Figure 14c, one would be overestimating the value of  $\Delta W^e$  for the case where the maximum and minimum stresses are both positive.

In the case where the maximum and minimum stresses are positive, or in a more general definition of the expression for  $\Delta W^e$  applicable to all values of  $R$  as long as  $\sigma_{max} > 0$ , it would be appropriate to represent the damage accumulation in the presence of the mean stress by using a simple functional form of a power law such as,

$$f\left(\frac{\sigma_m}{\sigma_a}\right) = \left(1 + \beta \frac{\sigma_m}{\sigma_a}\right)^{2m} \quad (36)$$

where:  $\beta \geq 0$  is a coefficient which characterizes the material sensitivity to mean stress,

and  $m \geq 0$  is a parameter related to the applied loading [41].

Therefore, the expression for  $\Delta W^e$  can now be written as,

$$\Delta W^e = \Delta W_{\sigma}^e \left( \frac{\sigma_m}{\sigma_a} \right) = \frac{\Delta \sigma^2}{8E} \left( 1 + \beta \frac{\sigma_m}{\sigma_a} \right)^{2m} \quad (37)$$

where:  $\Delta W_{\sigma}^e$  is the positive strain energy amplitude, i.e. for fully reversed loading with  $\sigma_m = 0$ ,  $R = -1$ , and  $\sigma_{max} = \Delta\sigma/2$ .  $\Delta W_{\sigma}^e$  is given by the first of equations 34.

In the case of the first of Equations 34,  $\beta = 1$  and  $m = 1$ . Replacing these values of  $\beta$  and  $m$  into Equation 37 we recover the expression for  $\Delta W^{e*}$  as shown in the first of Equations 34.

In Tables 5 and 6, the values of  $\sigma_{max}$  are calculated from Equation 17, and  $\sigma_{min} = \sigma_{max} - \Delta\sigma$ , where the values of  $\Delta\sigma$  are calculated from the second of Equations 32. The cyclic yield stress for A533-B1 steel is  $\sigma_0' = 345$  MPa, and for 4340 steel is  $\sigma_0' = 724$  MPa. It can be noticed from the tables that, the minimum stress  $\sigma_{min}$  values within the process zone have shown to be negative for all the cases analyzed, as shown in Tables 5 and 6. This permits that the expression for  $\Delta W^e$ , as given by the first of Equations 34, be used in the calculation of the total cyclic strain energy density.

#### 4.4 DERIVATION OF THE FATIGUE CRACK GROWTH MODEL

The derivation of the fatigue crack growth model is based on the same assumptions of Kujawski and Ellyin [1] for the cyclic stress and strain distribution within the plastic zone as shown in Figure 5. The difference is in the fact that Kujawski and Ellyin used a failure criterion based solely on the plastic component of the total cyclic strain energy  $\Delta W^p$ . For the proposed model the failure criterion is based on the total cyclic strain energy  $\Delta W^t$ .

Assuming that the plastic strain components at each point within the plastic zone remain proportional to each other, the expression for the cyclic stress range and the plastic strain range can be derived from Equation 32 and are expressed as follows,

$$\Delta\sigma = 2\sigma'_0 \left[ \frac{\Delta K^2}{4(1+n')\pi\sigma'^2_0 x} \right]^{\frac{n'}{n'+1}}, \quad (38)$$

$$\Delta\epsilon^p = \frac{2\sigma'_0}{E} \left[ \frac{\Delta K^2}{4(1+n')\pi\sigma'^2_0 x} \right]^{\frac{1}{n'+1}}$$

In terms of the product of the stress range and plastic strain range, Equations 38 reduces to,

$$\Delta\sigma\Delta\epsilon^p = \frac{\Delta K^2}{(1+n')\pi E x} \quad (39)$$

In the vicinity of the crack tip Equations 38 and 39 exhibit a singularity as  $x \rightarrow 0$ ,  $\Delta\sigma \rightarrow \infty$ ,  $\Delta\epsilon^p \rightarrow \infty$ ,  $\Delta\sigma\Delta\epsilon^p \rightarrow \infty$ . However, due to crack tip blunting and non-proportional plasticity within the process zone,  $\delta^*$ , immediately ahead of the crack tip, the stress and strain have a finite magnitude. The process zone is the region where the majority of the damage is experienced by the material.

The crack tip blunting radius,  $\rho_c$ , is associated with the threshold stress intensity range,  $\Delta K_{th}$ , below which crack propagation does not occur ( $da/dN \approx 0$ ).

Replacing  $x$  with  $(\delta^* + \rho_c)$  in Equation 39 we have,

$$\Delta \sigma \Delta \epsilon^p = \frac{\Delta K^2}{(1+n') \pi E (\delta' + \rho_c)} \quad (40)$$

Equation 35 for the total cyclic strain energy can be written in the following manner,

$$\Delta W^t = \Delta W^p + \Delta W^e = \frac{1-n'}{1+n'} \Delta \sigma \Delta \epsilon^p + \frac{\Delta \sigma^2}{8E} \left(1 + \frac{\sigma_m}{\sigma_a}\right)^2 \quad (41)$$

Rearranging we have,

$$\Delta W^t = \Delta \sigma \Delta \epsilon^p \left[ \frac{1-n'}{1+n'} + \frac{\Delta \sigma}{8E \Delta \epsilon^p} \left(1 + \frac{\sigma_m}{\sigma_a}\right)^2 \right] \quad (42)$$

Let,

$$\Psi = \frac{1-n'}{1+n'} + \frac{\Delta \sigma}{8E \Delta \epsilon^p} \left(1 + \frac{\sigma_m}{\sigma_a}\right)^2 \quad (43)$$

Therefore, Equation 42 can now be written as,

$$\Delta W^t = \Delta \sigma \Delta \epsilon^p \Psi \quad (44)$$

The number of cycles for the material to fail (or fracture) over the length  $(\delta' + \rho_c)$  at the specified stress and strain levels is obtained from [Ref. 14, Chapter 3],

$$\Delta W_f^t = \kappa (2N_f)^\alpha + \Delta W_0^t \quad (45)$$

where:  $\Delta W_0^t$  is a constant associated with the fatigue, or endurance, limit of the material. For most metals and for the lives up to  $2N_f < 5 \times 10^5$  this value is very small and it can

be ignored. Therefore, Equation 45 can be written in the form,

$$\Delta W_f^t = \kappa (2N_f)^\alpha \quad (46)$$

The term  $\Delta\sigma\Delta\epsilon^p$  on the right hand side of Equation 44 is obtained from Equation 40, and the term  $(2N_f)$  represents the number of reversals to failure ( $2N_f = 2\Delta N$ ). Therefore Equation 44 becomes,

$$\Delta W_f^t = \Delta\sigma\Delta\epsilon^p\Psi = \frac{\Delta K^2}{(1+n')\pi E(\delta^* + \rho_c)}\Psi \quad (47)$$

Let the number of cycles required to penetrate the process zone  $\delta^*$  be denoted by  $\Delta N$ . By equating Equations 46 and 47 we can calculate  $\Delta N$  as follows,

$$\kappa (2\Delta N)^\alpha = \frac{\Delta K^2}{(1+n')\pi E(\delta^* + \rho_c)}\Psi \quad (48)$$

Solving for  $(\delta^* + \rho_c)$  we have,

$$\delta^* + \rho_c = \frac{\Delta K^2}{(1+n')\pi E\kappa}\Psi (2\Delta N)^{-\alpha} \quad (49)$$

and solving for  $\delta^*$  we have,

$$\delta^* = \frac{\Delta K^2}{(1+n')\pi E\kappa}\Psi (2\Delta N)^{-\alpha} - \rho_c \quad (50)$$

Consequently, the crack extension per cycle can be determined from Equation 50 based on a condition of crack advance over a distance  $\delta^*$  which can be interpreted as an average



crack growth rate,  $da/dN = \delta^*/\Delta N$ , through the process zone as follows,

$$\frac{da}{dN} = \frac{\delta^*}{\Delta N} = \frac{\Delta K^2}{(1+n') \pi E \kappa} \Psi \frac{(2\Delta N)^{-\alpha}}{\Delta N} - \frac{\rho_c}{\Delta N} \quad (51)$$

The crack tip blunting radius  $\rho_c$  can be determined from Equation 51 noting that at the threshold value of the stress intensity factor range  $\Delta K$ , i.e.  $\Delta K = \Delta K_{th}$ , no crack growth will occur ( $da/dN \approx 0$ ). Therefore, solving for the crack tip blunting radius  $\rho_c$  we have,

$$\rho_c = \frac{\Delta K_{th}^2}{(1+n') \pi E \kappa} \Psi (2\Delta N)^{-\alpha} \quad (52)$$

Substituting Equation 52 into Equation 50 we can determine the size of the process zone  $\delta^*$ , which is given by the following expression,

$$\delta^* = \frac{\Delta K^2 - \Delta K_{th}^2}{(1+n') \pi E \kappa} \Psi (2\Delta N)^{-\alpha} \quad (53)$$

Raising both sides of Equation 53 to the power  $(-1/\alpha)$  we obtain,

$$\delta^{*-1/\alpha} = \left[ \frac{\Delta K^2 - \Delta K_{th}^2}{(1+n') \pi E \kappa} \Psi \right]^{-1/\alpha} (2\Delta N) \quad (54)$$

Multiplying both sides of Equation 54 by  $\delta^*$  and rearranging we obtain,

$$\delta^* = \delta \cdot \left[ \frac{\Delta K^2 - \Delta K_{th}^2}{(1+n') \pi E \kappa \delta^*} \Psi \right]^{-1/\alpha} (2\Delta N) \quad (55)$$

Dividing both sides of Equation 55 by  $(\Delta N)$ , and recalling that  $(\delta^*/\Delta N)$  represents the average crack growth per cycle, i.e.  $(\delta^*/\Delta N \approx da/dN)$  we obtain the proposed fatigue crack growth equation as,

$$\frac{\delta^*}{\Delta N} \approx \frac{da}{dN} = 2\delta^* \left[ \frac{\Delta K^2 - \Delta K_{th}^2}{(1+n') \pi E \kappa \delta^*} \Psi \right]^{-\frac{1}{\alpha}} \quad (56)$$

where:  $\Psi$  is given by Equation 43, and the values of  $\alpha$  and  $\kappa$  have yet to be determined.

Within the region of low cycles, or low reversals to failure, of the  $(\Delta W^t$  vs.  $2N_f)$  diagram, the value of  $\Delta W^t \approx \Delta W^p$ . Therefore Equation 41 becomes,

$$\Delta W^t = \Delta W^e + \Delta W^p \approx \Delta W^p = \frac{(1-n')}{(1+n')} \Delta \sigma \Delta \epsilon^p \quad (57)$$

The cyclic stress range  $\Delta \sigma$  and the cyclic plastic strain range  $\Delta \epsilon^p$  equations as a function of the number of cycles to failure ( $2N_f$ ) are given by [14],

$$\begin{aligned} \Delta \sigma &= 2\sigma'_f (2N_f)^b, \\ \Delta \epsilon^p &= 2\epsilon'_f (2N_f)^c \end{aligned} \quad (58)$$

Therefore, multiplying both Equations 58 we obtain,

$$\Delta \sigma \Delta \epsilon^p = 4\sigma'_f \epsilon'_f (2N_f)^{b+c} \quad (59)$$

Substituting Equation 59 into Equation 57 we have,

$$\Delta W^c = 4 \frac{(1-n')}{(1+n')} \sigma_f' \epsilon_f' (2N_f)^{b+c} \quad (60)$$

Combining Equations 46 and 60 we have,

$$\kappa (2N_f)^\alpha = 4 \frac{(1-n')}{(1+n')} \sigma_f' \epsilon_f' (2N_f)^{(b+c)} \quad (61)$$

Therefore, by similarity we obtain the values of  $\alpha$  and  $\kappa$  from Equation 61 as follows,

$$\kappa = 4 \frac{(1-n')}{(1+n')} \sigma_f' \epsilon_f' \quad (62)$$

and,

$$\alpha = b+c \quad (63)$$

Thus, Equation 56 can now be written as,

$$\frac{da}{dN} = 2\delta \cdot \left[ \frac{\Delta K^2 - \Delta K_{th}^2}{4\pi (1-n') \sigma_f' \epsilon_f' E \delta} \Psi \right]^{-\frac{1}{b+c}} \quad (64)$$

where:  $\sigma_f'$  is the fatigue strength coefficient,  $\epsilon_f'$  is the fatigue ductility coefficient,  $b$  is the fatigue strength exponent,  $c$  is the fatigue ductility exponent,  $n'$  is the cyclic strain

hardening exponent, and  $\Psi$  is given by Equation 43.

## **5.0 COMPARISON OF THE PROPOSED CRACK GROWTH MODEL WITH THE EXPERIMENTAL DATA**

The verification of the proposed model was based on a comparison with existing experimental data from the literature. The experimental data used included the one used by Kujawski and Ellyin [1] to test their model, and the addition of two aluminum alloys 2024-T3[42,43], and 7075-T6[42,43]. The data used by Kujawski and Ellyin comprises four cast steels (SAE 0050A, C-Mn, Mn-Mo, AISI 8630) [16], A533-B1 steel [17], and 4340 steel [18].

The values of the material parameter  $\delta^*$  were calculated by matching Equation 53 with the best fit curve through the experimental  $(da/dN)$  vs.  $\Delta K$  data at one value of  $\Delta K$  and  $(da/dN)$ . The value of  $\Delta K$  selected for the calculation of  $\delta^*$  was the one which would be located near the transition from Region I to Region II in the  $(da/dN)$  vs.  $\Delta K$  diagram.

The calculation of  $\delta^*$  can also be done by trial and error, in attempting to determine the best value of  $\delta^*$  which yield the best fit of Equation 64 through the experimental data.

Table 7 shows the values of the cyclic and fatigue properties for the six steel, and two aluminum alloys. Table 8 shows the values of the threshold stress intensity factors,  $\Delta K_{th}$ , and the calculated process zone sizes,  $\delta^*$ , for all of the alloys.

Tables 9 to 14 show the values calculated with the proposed model, Equation 64, the best fit values through the experimental data, and the values calculated with the model proposed by Kujawski and Ellyin (Equation 9) for the six steel alloys. The best fit through the experimental data was calculated based on the Least-Squares Polynomial Approximation.

The results calculated from Equation 64 are compared with the experimental data and plotted in Figures 15 to 20 as a function of the stress intensity factor range  $\Delta K$ .

Tables 15 and 16 show the values calculated with the proposed model, Equation 64, and the best fit through the experimental data points for the 7075-T6 and 2024-T3 aluminum alloys.

Equation 64 is compared with the experimental data in Figures 21 and 22 as a function of the stress intensity factor range,  $\Delta K$ , for the two aluminum alloys.

Table 17 shows the standard deviation of the proposed model, and Kujawski and Ellyin's model, compared with the best fit (Least-Squares polynomial) through the experimental data.

## **6.0 CONCLUSIONS**

A fatigue crack growth model has been developed which incorporates terms for the bulk cyclic and low cycle fatigue properties of the materials.

This model, described by Equation 64, was developed as an attempt to correct the model proposed by Kujawski and Ellyin [1], which tends to underestimate the effects of the mean stress, in the fatigue crack growth rate at low and intermediate stress intensities, and high values of the stress ratio.

From Figures 6 to 11, and Figures 15 to 20 one can see that the fit of the experimental data given by Equation 64 is better than the one given by Equation 9 for low and intermediate stress intensities, and for all values of  $R$  represented in the data.

The Standard Deviation ( $s$ ) between the results obtained by the proposed model, Equation 64, and Kujawski and Ellyin's model, Equation 9, when compared with the best fit through the experimental data using the Least-Squares Polynomial Method, are shown in Table 17. Only the results for the cast steel alloys are shown, since Kujawski and Ellyin did not compare Equation 9 with the experimental data for the two aluminum alloys. From Table 17 one can notice the better fit achieved by the proposed model.

The correlation of the results obtained with the proposed model and the experimental data for the two aluminum alloys in Region II of the  $(da/dN \text{ vs. } \Delta K)$  diagram follows the pattern indicated by Figure 2. This is related to the values of the cyclic strain hardening exponent  $n'$  in Equation 64, which seem to show a transition at around  $n' = 0.4$ . This parameter controls the spread between the curves, i.e. the greater the value of  $n'$ , the greater the spread between the curves. The exponent  $(-1/\alpha)$  composed of the fatigue strength exponent  $b$  and the fatigue ductility exponent  $c$ , in Equation 64 controls the shape of the curves, i.e. the curve tends to straighten the greater the value of the term  $-(b+c)$  gets.

Although a better fit yet could be achieved by calculating the value of the parameter  $\delta'$  for each set of experimental data points, i.e. for each value of the stress ratio,  $R$ , the equation would lose some of its generality in representing the entire spectrum of stress ratios for the material with a single constant value of the parameter  $\delta'$ .

## **7.0 REFERENCES**

- 1) D. Kujawski & F. Ellyin, A Fatigue Crack Growth Model With Load Ratio Effects, *Engineering Fracture Mechanics*, Vol. 28, No. 4, 367-378, 1987.
- 2) J. R. Rice, Mechanics of Crack Tip Deformation and Extension by Fatigue, *Fatigue Crack Propagation*, ASTM STP 415, 204-309, 1967.
- 3) D. T. Raske & JoDean Morrow, Mechanics of Materials in Low Cycle Fatigue Testing, *Manual on Low Cycle Fatigue Testing*, ASTM STP 465, 1-25, 1969.
- 4) A. K. Head, The Growth of Fatigue Cracks, *Philosophical Magazine*, 44, 925-938, 1953.
- 5) H. W. Liu & N. Iino, A Mechanical Model for Fatigue Crack Propagation, *Proceedings of the 2<sup>nd</sup> International Conference on Fracture*, 812-823, Chapman-Hall, 1969.
- 6) S. D. Anatolovich, A. Saxena & G. R. Chanani, A Model for Fatigue Crack Propagation, *Engineering Fracture Mechanics*, 7, 649-652, 1975.
- 7) D. Kujawski & F. Ellyin, A Fatigue Crack Propagation Model, *Engineering Fracture Mechanics*, 20, 695-704, 1984.
- 8) F. Ellyin, Crack Growth Rate Under Cyclic Loading and Effect of Different Singularity Fields, *Engineering Fracture Mechanics*, 25, 463-473, 1986.
- 9) J. W. Hutchinson, Singular Behaviour at the End of a Tensile Crack in a Hardening Material, *Journal of Mechanics and Physics of Solids*, 16, 13-31, 1968.
- 10) J. R. Rice & G. F. Rosengren, Plane Strain Deformation Near a Crack Tip in a Power-Law Hardening Material, *Journal of Mechanics and Physics of Solids*, 16, 1-12, 1968.
- 11) J. R. Rice, Stress due to a Sharp Notch in a Work-Hardening Elastic-Plastic Material Loaded by Longitudinal Shear, *Journal of Applied Mechanics*, 34, 287-298, 1967.
- 12) D. Kujawski and F. Ellyin, On the Size of the Plastic Zone Ahead of a Crack Tip, *Engineering Fracture Mechanics*, 25, 229-236, 1986.
- 13) F. A. McClintock, in *Fracture of Solids*, Drucker and Gilman, Eds., Wiley, New York, 65-102, 1963.

- 14) F. Ellyin, Class Notes for the Course "Mec.E.686, Fatigue of Engineering Materials", University of Alberta, Edmonton, Alberta, Fall 1991.
- 15) L. R. Kaisand and D. F. Mowbray, Relationships Between Low Cycle Fatigue and Fatigue Crack Growth Rate Properties. *Journal of Testing and Evaluation*, Vol. 7, No. 5, 270-280, September 1979.
- 16) R. I. Stephens et al., Constant and Variable Amplitude Fatigue Behaviour of Five Cast Steels at Room Temperature and -45°C, *Journal of Engineering Materials and Technology*, 106, 25-37, 1984.
- 17) P. C. Paris et al., Extensive Studies of Low Fatigue Crack Growth Rates in A533 and A508 steels, *Stress Analysis and Growth of Crack Part I*, ASTM STP 513, 141-176, 1972.
- 18) G. Glinka, A Notch Stress-Strain Analysis Approach to Fatigue Crack Growth, *Engineering Fracture Mechanics*, 21, 245-261, 1985.
- 19) W. Elber, The Significance of Fatigue Crack Closure, *Damage Tolerance in Aircraft Structures*, ASTM STP 486, 230-242, 1971.
- 20) Karl-Heinz Schwalbe, Some Aspects of Crack Propagation under Monotonic and Cyclic Load, *Engineering Fracture Mechanics*, 9, 547-556, 1977.
- 21) M. Klesnil and P. Lukas, Influence of Strength and Stress History on Growth and Stabilization of Fatigue Cracks, *Engineering Fracture Mechanics*, 4, 333-345, 1972.
- 22) J. C. Radon, A Model for Fatigue Crack Growth in a Threshold Region, *International Journal of Fatigue*, 4, 161-166, 1982.
- 23) J. D. Morrow, Cyclic Plastic Strain Energy and Fatigue of Metals, in *Internal Friction, Damping and Cyclic Plasticity*, ASTM STP 378, 45-84, 1965.
- 24) R. G. Forman, V. E. Kearney, and R. M. Engle, Numerical Analysis of Crack Propagation in Cyclic-Loaded Structures, *Journal of Basic Engineering*, Vol. 89, No. 3, 1967.
- 25) P. C. Paris and F. Erdogan, A Critical Analysis of Crack Propagation Laws, *Journal of Basic Engineering*, Vol. 85, No. 4, 1963.
- 26) B. R. Kirby and C. J. Beevers, Slow Fatigue Crack Growth and Threshold Behaviour in Air and Vacuum of Commercial Aluminum Alloys, *Fatigue of Engineering Materials and Structures*, Vol. 1, 203-215, 1979.



- 27) F. Ellyin and H. P. Li, **Fatigue Crack Growth in Large Specimens with Various Stress Ratios**, *Journal of Pressure Vessel Technology*, Vol. 106, No. 3, 255-260, 1984.
- 28) J. Masounave and J. P. Bailon, **The Dependence of the Threshold Stress Intensity Factor on the Cyclic Stress Ratio of the Fatigue of Ferritic-Perlitic Steels**, *Scripta Metallurgica*, Vol. 9, 723-730, 1975.
- 29) H. V. Staal and J. D. Elen, **Crack Closure and Influence of the Stress Ratio R on Fatigue Crack Growth in Type 304 Stainless Steel at Room Temperature**, *Engineering Fracture Mechanics*, Vol. 11, 275-283, 1979.
- 30) S. Usami and S. Shida, **Elastic-Plastic Analysis of the Fatigue Limit for a Material with Small Flaws**, *Fatigue of Engineering Materials and Structures*, Vol. 1, 471-481, 1979.
- 31) J. E. King, **Surface Damage and Near Threshold Fatigue Crack Growth in a Ni-Base Superalloy in Vacuum**, *Fatigue of Engineering Materials and Structures*, Vol. 5, No. 2, 177-188, 1982.
- 32) M. Klesnil and P. Lukas, **Effect of Stress Cycle Asymetry on Fatigue Crack Growth**, *Material Science and Engineering*, Vol. 9, 231-240, 1972.
- 33) C. J. Beevers, **Fatigue Crack Growth Characteristics at Low Stress Intensities of Metals and Alloys**, *Metal Science*, 362-367, Aug/Sept 1977.
- 34) K. Tanaka et al., **Fatigue Growth Threshold of Small Cracks**, *International Journal of Fracture*, Vol. 17, No. 5, 519-533, October 1981.
- 35) R. O. Ritchie, **Influence of Microstructure on Near Threshold Fatigue Crack Propagation in Ultra-High Strength Steel**, *Metal Science*, Vol. 11, 368-381, 1977.
- 36) J. Masounave and J. P. Bailon, **Effect of Grain Size on the Threshold Stress Intensity Factor in Fatigue of a Ferritic Steel**, *Scripta Metallurgica*, Vol. 10, 165-170, 1976.
- 37) M. Klesnil and P. Lukas, **Influence of Strength and Stress History on Growth and Stabilization of Fatigue Cracks**, *Engineering Fracture Mechanics*, Vol. 4, 77-92, 1972.
- 38) R. T. Davenport and R. Brook, **The Threshold Stress Intensity Range in Fatigue**, *Fatigue of Engineering Materials and Structures*, Vol. 1, 151-158, 1979.
- 39) W. Elber, **Fatigue Crack Closure Under Cyclic Tension**, *Engineering Fracture*

**Mechanics, Vol. 2, 37-45, 1970.**

- 40) J. Schijve, Fatigue Crack Closure: Observations and Technical Significance, in Mechanics of Fatigue Crack Closure, ASTM STP-982, 5-34, 1988.**
- 41) D. Kujawski and F. Ellyin, A Unified Approach to Mean Stress Effect on Fatigue Threshold Conditions, International Journal of Fatigue, Vol. 17, 101-106, 1995.**
- 42) C.H.R. Boller and T. Seeger, Materials Data for Cyclic Loading, Elsevier, Amsterdam, 1987.**
- 43) Anon., SAE J1099 Technical Report on Fatigue Properties, SAE Information Report, 1975.**
- 44) S. Suresh, Fatigue of Materials, Cambridge University Press, Great Britain, 1991.**

**APPENDIX - B**

**TABLES OF RESULTS**

**TABLE - 1:** Mean Stress Values Equivalent to the Best Fit Values of  $(da/dN)$  vs.  $\Delta K$  for A533-B1 Steel.

for:  $R = 0.1$

$\Delta K$ [MPa $\sqrt{m}$ ]	$(da/dN)_{K-E}$ [m/cycles]	$(da/dN)_{Best\ Fit}$ [m/cycles]	$(\sigma_m)_{K-E}$ [MPa]	$(\sigma_m)_{Best\ Fit}$ [MPa]
8.24	.805E-10	.349E-09	144.2	570.5
8.27	.882E-10	.364E-09	143.7	561.2
8.36	.113E-09	.410E-09	142.3	535.7
8.53	.169E-09	.508E-09	139.6	494.4
8.82	.282E-09	.692E-09	135.2	443.0
9.26	.497E-09	.102E-08	128.7	389.7
9.86	.884E-09	.158E-08	119.8	340.8
10.66	.157E-08	.251E-08	108.3	296.5
11.69	.272E-08	.401E-08	94.0	256.1
12.98	.465E-08	.639E-08	78.3	216.5
14.55	.784E-08	.100E-07	64.4	175.7
16.44	.131E-07	.155E-07	52.3	131.4
18.67	.216E-07	.234E-07	42.0	82.2
21.27	.352E-07	.348E-07	33.6	27.1
22.02	.400E-07	.385E-07	31.6	11.5

**TABLE - 1:** Mean Stress Values Equivalent to the Best Fit Values of (da/dN) vs.  $\Delta K$  for A533-B1 Steel (Continued).

for:  $R = 0.3$

$\Delta K$ [MPa $\sqrt{m}$ ]	(da/dN) <sub>K-E</sub> [m/cycles]	(da/dN) <sub>Best Fit</sub> [m/cycles]	( $\sigma_m$ ) <sub>K-E</sub> [MPa]	( $\sigma_m$ ) <sub>Best Fit</sub> [MPa]
6.10	.806E-10	.585E-09	197.0	666.3
6.13	.867E-10	.607E-09	196.6	661.8
6.22	.106E-09	.675E-09	195.3	648.9
6.39	.149E-09	.813E-09	192.8	626.4
6.68	.234E-09	.105E-08	188.8	595.2
7.11	.395E-09	.145E-08	182.9	556.4
7.71	.688E-09	.207E-08	174.8	512.1
8.50	.121E-08	.301E-08	164.3	463.7
9.52	.211E-08	.444E-08	151.2	411.2
10.80	.365E-08	.655E-08	135.6	354.6
12.36	.618E-08	.963E-08	116.3	293.1
14.23	.102E-07	.140E-07	91.4	226.1
16.44	.170E-07	.203E-07	71.3	152.7
19.02	.279E-07	.289E-07	55.5	72.2
21.15	.400E-07	.372E-07	46.3	8.6

**TABLE - 1:** Mean Stress Values Equivalent to the Best Fit Values of (da/dN) vs.  $\Delta K$  for A533-B1 Steel (Continued).

for:  $R = 0.5$

$\Delta K$ [MPa $\sqrt{m}$ ]	(da/dN) <sub>K-E</sub> [m/cycles]	(da/dN) <sub>Best Fit</sub> [m/cycles]	( $\sigma_m$ ) <sub>K-E</sub> [MPa]	( $\sigma_m$ ) <sub>Best Fit</sub> [MPa]
5.27	.802E-10	.602E-09	234.4	681.6
5.30	.858E-10	.630E-09	234.1	678.9
5.39	.104E-09	.713E-09	233.1	670.9
5.57	.143E-09	.879E-09	231.2	656.5
5.85	.220E-09	.116E-08	228.1	635.1
6.28	.365E-09	.161E-08	223.6	606.5
6.88	.635E-09	.231E-08	217.3	570.6
7.67	.112E-08	.334E-08	209.1	528.4
8.68	.198E-08	.484E-08	198.9	479.3
9.95	.346E-08	.699E-08	186.5	423.3
11.51	.598E-08	.101E-07	171.9	359.8
13.37	.987E-08	.144E-07	141.1	288.6
15.57	.160E-07	.203E-07	108.6	209.3
18.14	.262E-07	.284E-07	83.6	121.3
20.69	.400E-07	.377E-07	66.7	37.6

**TABLE - 1:** Mean Stress Values Equivalent to the Best Fit Values of  $(da/dN)$  vs.  $\Delta K$  for A533-B1 Steel (Continued).

for:  $R = 0.7$

$\Delta K$ [MPa $\sqrt{m}$ ]	$(da/dN)_{K-E}$ [m/cycles]	$(da/dN)_{Best\ Fit}$ [m/cycles]	$(\sigma_m)_{K-E}$ [MPa]	$(\sigma_m)_{Best\ Fit}$ [MPa]
3.91	.803E-10	.523E-09	289.2	682.3
3.94	.849E-10	.539E-09	289.1	679.5
4.03	.994E-10	.590E-09	288.7	671.4
4.20	.130E-09	.687E-09	288.0	656.7
4.48	.191E-09	.853E-09	286.7	633.6
4.91	.309E-09	.112E-08	284.7	600.7
5.50	.529E-09	.151E-08	281.8	557.6
6.28	.935E-09	.207E-08	277.7	503.7
7.28	.168E-08	.288E-08	272.3	437.4
8.54	.304E-08	.400E-08	265.3	357.7
10.07	.545E-08	.555E-08	256.9	264.1
11.91	.963E-08	.768E-08	246.9	155.6
14.09	.150E-07	.106E-07	190.9	31.5
16.62	.236E-07	.144E-07	143.7	-108.6
19.55	.379E-07	.196E-07	108.8	-265.2
19.91	.400E-07	.202E-07	105.4	-284.2

**TABLE - 1:** Mean Stress Values Equivalent to the Best Fit Values of (da/dN) vs.  $\Delta K$  for A533-B1 Steel (Continued).

for:  $R = 0.8$

$\Delta K$ [MPa $\sqrt{m}$ ]	$(da/dN)_{K-E}$ [m/cycles]	$(da/dN)_{Best\ Fit}$ [m/cycles]	$(\sigma_m)_{K-E}$ [MPa]	$(\sigma_m)_{Best\ Fit}$ [MPa]
3.78	.806E-10	.645E-09	329.5	715.8
3.81	.854E-10	.662E-09	329.6	712.8
3.90	.101E-09	.713E-09	329.7	704.0
4.07	.133E-09	.812E-09	329.9	688.4
4.35	.200E-09	.989E-09	330.2	664.5
4.77	.326E-09	.127E-08	330.4	632.8
5.36	.569E-09	.172E-08	330.3	593.3
6.15	.103E-08	.241E-08	329.7	546.4
7.16	.189E-08	.364E-08	328.3	491.9
8.41	.347E-08	.493E-08	326.1	429.9
9.95	.635E-08	.712E-08	322.8	359.4
11.79	.114E-07	.102E-07	318.3	280.1
13.97	.170E-07	.146E-07	250.4	191.7
16.51	.257E-07	.207E-07	187.9	93.3
19.42	.400E-07	.290E-07	142.3	-14.3



**TABLE - 2:** Mean Stress Values Equivalent to the Best Fit Values of (da/dN) vs.  $\Delta K$  for 4340 Steel.

for:  $R = 0.1$

$\Delta K$ [MPa $\sqrt{m}$ ]	$(da/dN)_{K-E}$ [m/cycles]	$(da/dN)_{Best\ Fit}$ [m/cycles]	$(\sigma_m)_{K-E}$ [MPa]	$(\sigma_m)_{Best\ Fit}$ [MPa]
9.09	.120E-08	.175E-09	52.8	-5263.0 <sup>1</sup>
9.10	.121E-08	.192E-09	52.7	-4842.6 <sup>1</sup>
9.16	.129E-08	.307E-09	52.1	-3135.7 <sup>1</sup>
9.32	.151E-08	.615E-09	50.6	-1538.3
9.65	.202E-08	.131E-08	47.6	-588.8
10.25	.307E-08	.270E-08	42.8	-121.3
11.24	.517E-08	.541E-08	36.5	93.1
12.76	.932E-08	.106E-07	29.2	182.1
14.97	.174E-07	.203E-07	22.1	207.1
18.04	.332E-07	.386E-07	16.0	195.6
22.20	.638E-07	.720E-07	11.1	158.0
27.66	.123E-06	.132E-06	7.6	97.6
34.67	.234E-06	.236E-06	5.1	16.6
43.50	.441E-06	.415E-06	3.4	-76.3
54.44	.817E-06	.727E-06	2.3	-152.9
58.62	.100E-05	.882E-06	2.0	-165.2

<sup>1</sup>Unrealistic values since their modulus is greater than  $\sigma_r$ .

**TABLE - 2:** Mean Stress Values Equivalent to the Best Fit Values of (da/dN) vs.  $\Delta K$  for 4340 Steel (Continued).

for:  $R = 0.5$

$\Delta K$ [MPa $\sqrt{m}$ ]	$(da/dN)_{K-E}$ [m/cycles]	$(da/dN)_{Best\ Fit}$ [m/cycles]	$(\sigma_m)_{K-E}$ [MPa]	$(\sigma_m)_{Best\ Fit}$ [MPa]
4.09	.148E-09	.929E-10	344.0	-222.1
4.10	.152E-09	.106E-09	343.5	-72.4
4.16	.178E-09	.196E-09	340.0	434.3
4.32	.253E-09	.437E-09	331.0	793.2
4.66	.440E-09	.971E-09	312.3	937.1
5.27	.846E-09	.202E-08	257.1	953.0
6.27	.173E-08	.402E-08	189.7	899.4
7.81	.368E-08	.777E-08	129.3	805.5
10.04	.798E-08	.149E-07	83.3	691.6
13.17	.174E-07	.290E-07	51.9	575.5
17.38	.378E-07	.569E-07	32.0	471.8
22.92	.807E-07	.112E-06	19.7	388.2
30.02	.168E-06	.221E-06	12.3	324.3
38.97	.340E-06	.427E-06	7.8	273.8
49.80	.658E-06	.794E-06	5.1	228.3

**TABLE - 3:** Cyclic Strain Components as a function of  $\Delta K$  for A533-B1 Steel.

for:  $R = 0.1$

$\Delta K$ [MPa $\sqrt{m}$ ]	$\Delta\epsilon^e$ [m/m]	$\Delta\epsilon^p$ [m/m]	$\Delta\epsilon$ [m/m]
8.24	.3019E-02	.1536E-02	.4555E-02
8.27	.3022E-02	.1546E-02	.4568E-02
8.36	.3031E-02	.1575E-02	.4606E-02
8.53	.3049E-02	.1632E-02	.4681E-02
8.82	.3078E-02	.1728E-02	.4806E-02
9.26	.3120E-02	.1877E-02	.4997E-02
9.86	.3176E-02	.2091E-02	.5267E-02
10.66	.3248E-02	.2392E-02	.5640E-02
11.69	.3334E-02	.2802E-02	.6136E-02
12.98	.3434E-02	.3354E-02	.6788E-02
14.55	.3547E-02	.4080E-02	.7627E-02
16.44	.3671E-02	.5029E-02	.8700E-02
18.67	.3806E-02	.6256E-02	.1006E-02
21.27	.3949E-02	.7825E-02	.1177E-02
22.02	.3988E-02	.8305E-02	.1229E-02

**TABLE - 3:** Cyclic Strain Components as a Function of  $\Delta K$  for A533-B1 Steel  
(Continued).

for:  $R = 0.3$

$\Delta K$ [MPa $\sqrt{m}$ ]	$\Delta\varepsilon^c$ [m/m]	$\Delta\varepsilon^p$ [m/m]	$\Delta\varepsilon$ [m/m]
6.10	.2772E-02	.9155E-03	.3687E-02
6.13	.2776E-02	.9233E-03	.3699E-02
6.22	.2787E-02	.9467E-03	.3734E-02
6.39	.2809E-02	.9929E-03	.3802E-02
6.68	.2844E-02	.1070E-02	.3914E-02
7.11	.2895E-02	.1191E-02	.4086E-02
7.71	.2962E-02	.1369E-02	.4331E-02
8.50	.3046E-02	.1620E-02	.4666E-02
9.52	.3145E-02	.1970E-02	.5116E-02
10.80	.3259E-02	.2444E-02	.5704E-02
12.36	.3386E-02	.3082E-02	.6468E-02
14.23	.3524E-02	.3925E-02	.7449E-02
16.44	.3671E-02	.5029E-02	.8700E-02
19.02	.3826E-02	.6459E-02	.1028E-02
21.15	.3943E-02	.7750E-02	.1169E-02

**TABLE - 3:** Cyclic Strain Components as a Function of  $\Delta K$  for A533-B1 Steel  
(Continued).

for:  $R = 0.5$

$\Delta K$ [MPa $\sqrt{m}$ ]	$\Delta\epsilon^e$ [m/m]	$\Delta\epsilon^p$ [m/m]	$\Delta\epsilon$ [m/m]
5.27	.2660E-02	.7132E-03	.3373E-02
5.30	.2664E-02	.7202E-03	.3384E-02
5.39	.2677E-02	.7413E-03	.3418E-02
5.57	.2701E-02	.7831E-03	.3484E-02
5.85	.2740E-02	.8532E-03	.3593E-02
6.28	.2795E-02	.9624E-03	.3757E-02
6.88	.2868E-02	.1126E-02	.3994E-02
7.67	.2958E-02	.1357E-02	.4315E-02
8.68	.3064E-02	.1681E-02	.4746E-02
9.95	.3185E-02	.2125E-02	.5310E-02
11.51	.3319E-02	.2727E-02	.6045E-02
13.37	.3463E-02	.3529E-02	.6992E-02
15.57	.3616E-02	.4583E-02	.8199E-02
18.14	.3775E-02	.5957E-02	.9732E-02
20.69	.3918E-02	.7462E-02	.1138E-01

**TABLE - 3:** Cyclic Strain Components as a Function of  $\Delta K$  for A533-B1 Steel  
(Continued).

for:  $R = 0.7$

$\Delta K$ [MPa $\sqrt{m}$ ]	$\Delta\varepsilon^e$ [m/m]	$\Delta\varepsilon^p$ [m/m]	$\Delta\varepsilon$ [m/m]
3.91	.2444E-02	.4274E-03	.2871E-02
3.94	.2450E-02	.4329E-03	.2882E-02
4.03	.2465E-02	.4500E-03	.2915E-02
4.20	.2494E-02	.4831E-02	.2977E-02
4.48	.2540E-02	.5397E-03	.3080E-02
4.91	.2606E-02	.6305E-03	.3237E-02
5.50	.2692E-02	.7663E-03	.3458E-02
6.28	.2795E-02	.9624E-03	.3757E-02
7.28	.2915E-02	.1242E-02	.4157E-02
8.54	.3050E-02	.1634E-02	.4683E-02
10.07	.3196E-02	.2170E-02	.5365E-02
11.91	.3351E-02	.2894E-02	.6245E-02
14.09	.3514E-02	.3859E-02	.7373E-02
16.62	.3683E-02	.5126E-02	.8809E-02
19.55	.3856E-02	.6771E-02	.1063E-01
19.91	.3876E-02	.6986E-02	.1086E-01

**TABLE - 3:** Cyclic Strain Components as a Function of  $\Delta K$  for A533-B1 Steel (Continued).

for:  $R = 0.8$

$\Delta K$ [MPa $\sqrt{m}$ ]	$\Delta\varepsilon^c$ [m/m]	$\Delta\varepsilon^p$ [m/m]	$\Delta\varepsilon$ [m/m]
3.78	.2420E-02	.4022E-03	.2822E-02
3.81	.2425E-02	.4077E-03	.2833E-02
3.90	.2442E-02	.4244E-03	.2866E-02
4.07	.2471E-02	.4567E-03	.2928E-02
4.35	.2519E-02	.5131E-03	.3032E-02
4.77	.2586E-02	.6010E-03	.3187E-02
5.36	.2673E-02	.7343E-03	.3407E-02
6.15	.2778E-02	.9284E-03	.3707E-02
7.16	.2901E-02	.1206E-02	.4106E-02
8.41	.3036E-02	.1591E-02	.4627E-02
9.95	.3185E-02	.2124E-02	.5308E-02
11.79	.3342E-02	.2844E-02	.6185E-02
13.97	.3506E-02	.3802E-02	.7308E-02
16.51	.3676E-02	.5068E-02	.8744E-02
19.42	.3849E-02	.6693E-02	.1054E-01

**TABLE - 4:** Cyclic Strain Components as a Function of  $\Delta K$  for 4340 Steel.

for:  $R = 0.1$

$\Delta K$ [MPa $\sqrt{m}$ ]	$\Delta\varepsilon^e$ [m/m]	$\Delta\varepsilon^p$ [m/m]	$\Delta\varepsilon$ [m/m]
9.09	.8604E-02	.3055E-01	.3916E-01
9.10	.8606E-02	.3061E-01	.3921E-01
9.16	.8621E-02	.3096E-01	.3958E-01
9.32	.8658E-02	.3188E-01	.4054E-01
9.65	.8735E-02	.3388E-01	.4262E-01
10.25	.8870E-02	.3764E-01	.4651E-01
11.24	.9081E-02	.4422E-01	.5330E-01
12.76	.9380E-02	.5518E-01	.6456E-01
14.97	.9769E-02	.7291E-01	.8267E-01
18.04	.1025E-01	.1010	.1113
22.20	.1080E-01	.1451	.1559
27.66	.1142E-01	.2130	.2244
34.67	.1210E-01	.3159	.3280
43.50	.1282E-01	.4693	.4821
54.44	.1357E-01	.6941	.7077
58.62	.1383E-01	.7897	.8037



**TABLE - 4:** Cyclic Strain Components as a Function of  $\Delta K$  for 4340 Steel (Continued).

for:  $R = 0.5$

$\Delta K$ [MPa $\sqrt{m}$ ]	$\Delta \epsilon^e$ [m/cycles]	$\Delta \epsilon^p$ [m/cycles]	$\Delta \epsilon$ [MPa]
4.09	.7020E-02	.7583E-02	.1460E-01
4.10	.7024E-02	.7613E-02	.1464E-01
4.16	.7050E-02	.7808E-02	.1486E-01
4.32	.7118E-02	.8336E-02	.1545E-01
4.66	.7255E-02	.9500E-02	.1676E-01
5.27	.7486E-02	.1177E-01	.1926E-01
6.27	.7826E-02	.1596E-01	.2378E-01
7.81	.8276E-02	.2341E-01	.3168E-01
10.04	.8825E-02	.3634E-01	.4517E-01
13.17	.9455E-02	.5830E-01	.6775E-01
17.38	.1015E-01	.9465E-01	.1048
22.92	.1089E-01	.1533	.1642
30.02	.1166E-01	.2456	.2573
38.97	.1247E-01	.3873	.3998
49.80	.1327E-01	.5942	.6075

**TABLE 5:** Maximum and minimum stresses within the process zone as a function of  $\Delta K$  for A533-B1 steel.

for:  $R = 0.1$

$\Delta K$ [MPa $\sqrt{m}$ ]	$\sigma_{max}$ [MPa]	$\sigma_{min}$ [MPa]
8.20	617.0	-230.2
8.22	617.4	-230.4
8.29	618.9	-230.9
8.42	621.6	-231.9
8.63	626.1	-233.6
8.95	632.6	-236.0
9.40	641.4	-239.3
10.00	652.8	-243.5
10.77	666.6	-248.7
11.73	682.9	-254.8
12.90	701.6	-261.7
14.31	722.4	-269.5
15.97	745.2	-278.0
17.90	769.7	-287.2
20.14	795.8	-296.9

**TABLE 5:** Maximum and minimum stresses within the process zone as a function of  $\Delta K$  for A533-B1 steel (Continued).

for:  $R = 0.3$

$\Delta K$ [MPa $\sqrt{m}$ ]	$\sigma_{max}$ [MPa]	$\sigma_{min}$ [MPa]
6.10	567.3	-185.4
6.12	567.8	-185.6
6.18	569.5	-186.1
6.31	572.9	-187.2
6.53	578.3	-189.0
6.84	586.1	-191.6
7.29	596.6	-195.0
7.88	610.0	-199.4
8.63	626.1	-204.6
9.58	644.8	-210.7
10.73	665.9	-217.6
12.12	689.2	-225.3
13.76	714.4	-233.5
15.67	741.2	-242.3

**TABLE 5:** Maximum and minimum stresses within the process zone as a function of  $\Delta K$  for A533-B1 steel (Continued).

for: R = 0.5

$\Delta K$ [MPa $\sqrt{m}$ ]	$\sigma_{max}$ [MPa]	$\sigma_{min}$ [MPa]
5.33	546.0	-141.7
5.35	546.5	-141.8
5.41	548.4	-142.3
5.54	552.1	-143.3
5.75	558.0	-144.8
6.07	566.5	-147.0
6.51	577.8	-150.0
7.09	592.1	-153.7
7.84	609.2	-158.1
8.78	629.0	-163.3
9.92	651.3	-169.0
11.30	675.7	-175.3
12.92	701.8	-182.1
14.81	729.5	-189.3
16.99	758.5	-196.8

**TABLE 5:** Maximum and minimum stresses within the process zone as a function of  $\Delta K$  for A533-B1 steel (Continued).

for:  $R = 0.7$

$\Delta K$ [MPa $\sqrt{m}$ ]	$\sigma_{max}$ [MPa]	$\sigma_{min}$ [MPa]
4.04	504.7	-72.8
4.06	505.4	-72.9
4.12	507.7	-73.2
4.25	512.0	-73.9
4.45	518.9	-74.8
4.76	528.9	-76.3
5.19	542.0	-78.2
5.76	558.2	-80.5
6.50	577.6	-83.3
7.42	599.6	-86.5
8.53	624.0	-90.0
9.87	650.3	-93.8
11.46	678.4	-97.9

**TABLE 5:** Maximum and minimum stresses within the process zone as a function of  $\Delta K$  for A533-B1 steel (Continued).

for: R = 0.8

$\Delta K$ [MPa $\sqrt{m}$ ]	$\sigma_{max}$ [MPa]	$\sigma_{min}$ [MPa]
4.15	508.6	-20.4
4.17	509.3	-20.4
4.23	511.5	-20.5
4.35	515.6	-20.7
4.56	522.3	-20.9
4.86	532.0	-21.3
5.28	544.7	-21.8
5.85	560.6	-22.5
6.57	579.4	-23.2
7.47	600.9	-24.1
8.57	624.8	-25.0
9.90	650.8	-26.1

**TABLE 6:** Maximum and minimum stresses within the process zone as a function of  $\Delta K$  for 4340 steel.  
for:  $R = 0.1$

$\Delta K$ [MPa $\sqrt{m}$ ]	$\sigma_{\max}$ [MPa]	$\sigma_{\min}$ [MPa]
9.01	1044.1	-659.7
9.02	1044.4	-659.9
9.08	1046.2	-661.0
9.24	1050.7	-663.9
9.57	1060.2	-669.8
10.17	1076.8	-680.3
11.16	1102.6	-696.6
12.68	1139.1	-719.7
14.89	1186.7	-749.8
17.98	1245.1	-786.6
22.14	1312.9	-829.5
27.61	1388.8	-877.5
34.63	1471.4	-929.6
43.47	1559.1	-985.1
54.42	1651.0	-1043.1
67.80	1746.1	-1103.2

**TABLE 6:** Maximum and minimum stresses within the process zone as a function of  $\Delta K$  for 4340 steel (Continued).  
for:  $R = 0.5$

$\Delta K$ [MPa $\sqrt{m}$ ]	$\sigma_{max}$ [MPa]	$\sigma_{min}$ [MPa]
4.01	987.0	-399.6
4.02	987.5	-399.8
4.08	991.3	-401.3
4.24	1001.0	-405.2
4.58	1020.6	-413.2
5.19	1053.6	-426.5
6.19	1102.2	-446.2
7.73	1166.5	-472.2
9.97	1244.6	-503.9
13.10	1334.2	-540.1
17.32	1432.6	-579.9
22.86	1537.5	-622.4
29.98	1647.4	-666.9
38.94	1760.9	-712.9
50.04	1877.1	-759.9
53.54	1909.8	-773.2



**TABLE - 7: Material's Cyclic and Fatigue Properties.**

Alloy	E [GPa]	$\sigma_0$ [MPa]	n'	$\sigma'_f$ [MPa]	$\epsilon'_f$	c	b
0050A	209	400	.171	1337	.30	-.569	-.127
C-Mn	208	372	.141	868	.15	-.514	-.101
Mn-Mo	211	427	.096	1116	.78	-.729	-.101
8630	207	682	.122	1936	.42	-.693	-.121
A533-B1	200	345	.165	869	.32	-.520	-.085
4340	209	724	.146	1713	.83	-.650	-.095
7075-T6	71	524	.470	1317	.19	-.400	-.200
2024-T3	74	378	.400	314	.162	-.452	-.091

**TABLE - 8:** Threshold Stress Intensity Factors  $\Delta K_{th}$  [MPa  $\sqrt{m}$ ] as a function of R, and process zone sizes  $\delta^*$ .

Alloy	R=0	R=.1	R=.2	R=.3	R=.33	R=.5	R=.7	R=.8	$\delta^*$ [m]
0050A	13	-	-	-	-	10	-	-	4.0E-05
C-Mn	13	-	-	-	-	9	-	-	2.0E-03
Mn-Mo	14	-	-	-	-	11	-	-	2.0E-04
8630	13	-	-	-	-	10	-	-	1.0E-04
A533-B1	-	7.7	-	5.4	-	4.5	2.9	2.8	1.5E-04
4340	-	7.8	-	-	-	3.6	-	-	1.5E-06
7075-T6	3.5	-	2.8	-	2.7	2.5	1.9	1.3	.75E-07
2024-T3	2.7	-	-	-	2.1	1.9	1.7	-	.55E-04

**TABLE - 9:** Comparison of (da/dN) vs. ΔK values for A533-B1 steel. Equation 9 (Kujawski-Ellyin), best fit, and the proposed Equation 64.  
for: R = 0.1

ΔK [MPa√m]	(da/dN) <sub>EQ. 11</sub> [m/cycles]	(da/dN) <sub>Best Fit</sub> [m/cycles]	(da/dN) <sub>EQ. 64</sub> [m/cycles]
8.31	.100E-09	.386E-09	.136E-09
8.33	.106E-09	.397E-09	.143E-09
8.40	.125E-09	.431E-09	.168E-09
8.53	.167E-09	.505E-09	.223E-09
8.74	.248E-09	.638E-09	.327E-09
9.06	.394E-09	.865E-09	.510E-09
9.51	.646E-09	.124E-08	.820E-09
10.10	.107E-08	.184E-08	.133E-08
10.87	.177E-08	.278E-08	.214E-08
11.82	.289E-08	.422E-08	.342E-08
12.98	.464E-08	.638E-08	.538E-08
14.37	.743E-08	.957E-08	.840E-08
16.02	.118E-07	.142E-07	.130E-07
17.94	.185E-07	.207E-07	.200E-07
20.16	.289E-07	.297E-07	.304E-07
22.02	.400E-07	.385E-07	.415E-07

**TABLE - 9:** Comparison of (da/dN) vs.  $\Delta K$  values for A533-B1 steel. Equation 9 (Kujawski-Ellyin), best fit, and the proposed Equation 64 (Continued).

for:  $R = 0.3$

$\Delta K$ [MPa $\sqrt{m}$ ]	(da/dN) <sub>EQ. 11</sub> [m/cycles]	(da/dN) <sub>Best Fit</sub> [m/cycles]	(da/dN) <sub>EQ. 64</sub> [m/cycles]
7.35	.502E-09	.169E-08	.764E-09
7.37	.512E-09	.171E-08	.777E-09
7.43	.541E-09	.177E-08	.816E-09
7.54	.599E-09	.189E-08	.894E-09
7.74	.705E-09	.210E-08	.103E-08
8.03	.879E-09	.243E-08	.125E-08
8.43	.116E-08	.293E-08	.160E-08
8.97	.159E-08	.364E-08	.212E-08
9.66	.225E-08	.465E-08	.288E-08
10.52	.327E-08	.607E-08	.402E-08
11.58	.482E-08	.802E-08	.571E-08
12.84	.711E-08	.107E-07	.820E-08
14.34	.105E-07	.143E-07	.119E-07
16.08	.157E-07	.192E-07	.174E-07
17.25	.200E-07	.228E-07	.218E-07

**TABLE - 9:** Comparison of (da/dN) vs.  $\Delta K$  values for A533-B1 steel. Equation 9 (Kujawski-Ellyin), best fit, and the proposed Equation 64 (Continued).  
for:  $R = 0.5$

$\Delta K$ [MPa $\sqrt{m}$ ]	(da/dN) <sub>EQ. 11</sub> [m/cycles]	(da/dN) <sub>Best Fit</sub> [m/cycles]	(da/dN) <sub>EQ. 64</sub> [m/cycles]
5.38	.101E-09	.699E-09	.227E-09
5.40	.105E-09	.718E-09	.236E-09
5.46	.119E-09	.779E-09	.263E-09
5.59	.149E-09	.903E-09	.321E-09
5.80	.205E-09	.111E-08	.423E-09
6.11	.304E-09	.143E-08	.592E-09
6.55	.479E-09	.192E-08	.866E-09
7.14	.778E-09	.264E-08	.129E-08
7.88	.128E-08	.364E-08	.194E-08
8.81	.211E-08	.505E-08	.292E-08
9.95	.346E-08	.699E-08	.441E-08
11.32	.564E-08	.967E-08	.668E-08
12.94	.890E-08	.133E-07	.101E-07
14.83	.137E-07	.182E-07	.154E-07
17.00	.213E-07	.247E-07	.234E-07
18.92	.300E-07	.311E-07	.325E-07

**TABLE - 9:** Comparison of  $(da/dN)$  vs.  $\Delta K$  values for A533-B1 steel. Equation 9 (Kujawski-Ellyin), best fit, and the proposed Equation 64 (Continued).  
for:  $R = 0.7$

$\Delta K$ [MPa $\sqrt{m}$ ]	$(da/dN)_{EQ. 11}$ [m/cycles]	$(da/dN)_{Best Fit}$ [m/cycles]	$(da/dN)_{EQ. 64}$ [m/cycles]
4.04	.100E-09	.593E-09	.419E-09
4.06	.104E-09	.604E-09	.430E-09
4.12	.115E-09	.641E-09	.465E-09
4.25	.139E-09	.714E-09	.534E-09
4.45	.184E-09	.835E-09	.653E-09
4.76	.265E-09	.103E-08	.845E-09
5.19	.406E-09	.130E-08	.114E-08
5.76	.651E-09	.170E-08	.157E-08
6.50	.108E-08	.224E-08	.220E-08
7.42	.180E-08	.299E-08	.314E-08
8.53	.303E-08	.400E-08	.452E-08
9.87	.508E-08	.534E-08	.659E-08
11.46	.846E-08	.713E-08	.971E-08
12.05	.100E-07	.785E-08	.111E-7

**TABLE - 9:** Comparison of (da/dN) vs.  $\Delta K$  values for A533-B1 steel. Equation 9 (Kujawski-Ellyin), best fit, and the proposed Equation 64 (Continued).

for:  $R = 0.8$

$\Delta K$ [MPa $\sqrt{m}$ ]	(da/dN) <sub>EQ.11</sub> [m/cycles]	(da/dN) <sub>Best Fit</sub> [m/cycles]	(da/dN) <sub>EQ. 64</sub> [m/cycles]
5.22	.502E-09	.161E-08	.157E-08
5.23	.508E-09	.162E-08	.159E-08
5.29	.536E-09	.167E-08	.164E-08
5.41	.591E-09	.176E-08	.175E-08
5.59	.687E-09	.191E-08	.192E-08
5.87	.848E-09	.215E-08	.219E-08
6.26	.111E-08	.251E-08	.260E-08
6.78	.153E-08	.303E-08	.318E-08
7.45	.220E-08	.375E-08	.401E-08
8.28	.328E-08	.477E-08	.519E-08
9.29	.499E-08	.614E-08	.686E-08
10.51	.771E-08	.802E-08	.925E-08
11.34	.100E-07	.943E-08	.111E-07

**TABLE - 10:** Comparison of  $(da/dN)$  vs.  $\Delta K$  values for 4340 steel. Equation 9 (Kujawski-Ellyin), best fit, and the proposed Equation 64. for:  $R = 0.1$

$\Delta K$ [MPa $\sqrt{m}$ ]	$(da/dN)_{EQ. 11}$ [m/cycles]	$(da/dN)_{Best Fit}$ [m/cycles]	$(da/dN)_{EQ. 64}$ [m/cycles]
9.01	.109E-08	.225E-10	.143E-08
9.02	.111E-08	393E-10	.145E-08
9.08	.118E-08	.152E-09	.155E-08
9.24	.140E-08	.454E-09	.183E-08
9.57	.189E-08	.113E-08	.247E-08
10.17	.292E-08	.251E-08	.381E-08
11.16	.499E-08	.518E-08	.649E-08
12.68	.908E-08	.103E-07	.118E-07
14.89	.171E-07	.200E-07	.221E-07
17.98	.328E-07	.381E-07	.422E-07
22.14	.633E-07	.715E-07	.811E-07
27.61	.122E-06	.131E-06	.156E-06
34.63	.233E-06	.235E-06	.297E-06
43.47	.440E-06	.414E-06	.560E-06
54.42	.816E-06	.726E-06	.104E-05
58.62	.100E-05	.882E-06	.127E-05



**TABLE - 10:** Comparison of  $(da/dN)$  vs.  $\Delta K$  values for 4340 steel. Equation 9 (Kujawski-Ellyin), best fit, and the proposed Equation 64 (Continued).  
for:  $R = 0.5$

$\Delta K$ [MPa $\sqrt{m}$ ]	$(da/dN)_{EQ. 11}$ [m/cycles]	$(da/dN)_{Best Fit}$ [m/cycles]	$(da/dN)_{EQ. 64}$ [m/cycles]
4.01	.116E-09	.230E-10	.148E-09
4.02	.120E-09	.352E-10	.153E-09
4.08	.144E-09	.117E-09	.183E-09
4.24	.215E-09	.340E-09	.272E-09
4.58	.393E-09	.838E-09	.492E-09
5.19	.789E-09	.184E-08	.996E-09
6.19	.165E-08	.377E-08	.212E-08
7.73	.357E-08	.748E-08	.461E-08
9.97	.782E-08	.147E-07	.101E-07
13.10	.172E-07	.287E-07	.222E-07
17.32	.375E-07	.565E-07	.482E-07
22.86	.802E-07	.112E-06	.103E-06
29.98	.167E-06	.219E-06	.214E-06
38.94	.339E-06	.426E-06	.432E-06
50.04	.667E-06	.804E-06	.849E-06
55.94	.900E-06	.106E-05	.115E-05

**TABLE - 11:** Comparison of  $(da/dN)$  vs.  $\Delta K$  values for AISI 8630 cast steel. Equation 9 (Kujawski-Ellyin), best fit, and the proposed Equation 64.  
for:  $R = 0$

$\Delta K$ [MPa $\sqrt{m}$ ]	$(da/dN)_{EQ. 11}$ [m/cycles]	$(da/dN)_{Best Fit}$ [m/cycles]	$(da/dN)_{EQ. 64}$ [m/cycles]
14.10	.204E-08	.415E-08	.533E-08
14.18	.223E-08	.434E-08	.581E-08
14.46	.294E-08	.505E-08	.759E-08
15.00	.444E-08	.659E-08	.113E-07
15.86	.716E-08	.951E-08	.178E-07
17.18	.121E-07	.151E-07	.292E-07
19.00	.204E-07	.247E-07	.475E-07
21.44	.341E-07	.408E-07	.766E-07
24.56	.562E-07	.656E-07	.122E-06
28.44	.911E-07	.101E-06	.191E-06
33.20	.146E-06	.147E-06	.297E-06
38.92	.231E-06	.209E-06	.458E-06
45.66	.359E-06	.302E-06	.697E-06
53.52	.545E-06	.475E-06	.105E-05
62.60	.789E-06	.819E-06	.156E-05
69.34	.100E-05	.118E-05	.202E-05

**TABLE - 11:** Comparison of (da/dN) vs.  $\Delta K$  values for AISI 8630 cast steel. Equation 9 (Kujawski-Ellyin), best fit, and the proposed Equation 64 (Continued).

for:  $R = 0.5$

$\Delta K$ [MPa $\sqrt{m}$ ]	(da/dN) <sub>EQ. 11</sub> [m/cycles]	(da/dN) <sub>Best Fit</sub> [m/cycles]	(da/dN) <sub>EQ. 64</sub> [m/cycles]
11.26	.204E-08	.325E-08	.581E-08
11.34	.221E-08	.390E-08	.627E-08
11.62	.284E-08	.602E-08	.792E-08
12.14	.414E-08	.951E-08	.112E-07
13.02	.666E-08	.144E-07	.172E-07
14.32	.111E-07	.205E-07	.271E-07
16.14	.189E-07	.288E-07	.432E-07
18.58	.323E-07	.425E-07	.687E-07
21.68	.542E-07	.656E-07	.108E-06
25.58	.905E-07	.102E-06	.170E-06
30.32	.143E-06	.158E-06	.265E-06
36.02	.224E-06	.271E-06	.410E-06
42.74	.342E-06	.503E-06	.629E-06
45.56	.400E-06	.594E-06	.736E-06

**TABLE - 12:** Comparison of (da/dN) vs.  $\Delta K$  values for C-Mn cast steel. Equation 9 (Kujawski-Ellyin), best fit, and the proposed Equation 64.

for:  $R = 0$

$\Delta K$ [MPa $\sqrt{m}$ ]	(da/dN) <sub>EQ. 11</sub> [m/cycles]	(da/dN) <sub>Best Fit</sub> [m/cycles]	(da/dN) <sub>EQ. 64</sub> [m/cycles]
15.18	.200E-08	.403E-07	.509E-08
15.26	.213E-08	.410E-07	.538E-08
15.54	.263E-08	.434E-07	.641E-08
16.06	.368E-08	.481E-07	.848E-08
16.92	.580E-08	.566E-07	.123E-07
18.2	.990E-08	.712E-07	.186E-07
20.00	.178E-07	.958E-07	.289E-07
22.38	.317E-07	.137E-06	.448E-07
25.44	.549E-07	.205E-06	.693E-07
29.26	.941E-07	.321E-06	.107E-06
33.94	.159E-06	.518E-06	.166E-06
39.54	.265E-06	.851E-06	.257E-06
46.16	.440E-06	.141E-05	.400E-06
53.88	.733E-06	.236E-05	.625E-06
59.22	.100E-05	.323E-05	.822E-06

**TABLE - 12:** Comparison of (da/dN) vs.  $\Delta K$  values for C-Mn cast steel. Equation 9 (Kujawski-Ellyin), best fit, and the proposed Equation 64 (Continued).

for:  $R = 0.5$

$\Delta K$ [MPa $\sqrt{m}$ ]	(da/dN) <sub>EQ. 11</sub> [m/cycles]	(da/dN) <sub>Best Fit</sub> [m/cycles]	(da/dN) <sub>EQ. 64</sub> [m/cycles]
13.20	.501E-08	.634E-08	.192E-07
13.28	.519E-08	.673E-08	.197E-07
13.54	.580E-08	.799E-08	.213E-07
14.04	.708E-08	.105E-07	.245E-07
14.88	.954E-08	.147E-07	.299E-07
16.12	.139E-07	.212E-07	.384E-07
17.84	.216E-07	.310E-07	.511E-07
20.14	.350E-07	.458E-07	.698E-07
23.10	.583E-07	.688E-07	.972E-07
26.78	.977E-07	.106E-06	.137E-06
31.30	.164E-06	.168E-06	.198E-06
36.70	.274E-06	.273E-06	.289E-06
37.76	.300E-06	.298E-06	.310E-06

**TABLE - 13:** Comparison of  $(da/dN)$  vs.  $\Delta K$  values for Mn-Mo cast steel. Equation 9 (Kujawski-Ellyin), best fit, and the proposed Equation 64.

for:  $R = 0$

$\Delta K$ [MPa $\sqrt{m}$ ]	$(da/dN)_{EQ. 11}$ [m/cycles]	$(da/dN)_{Best Fit}$ [m/cycles]	$(da/dN)_{EQ. 64}$ [m/cycles]
15.02	.307E-08	.586E-08	.466E-08
15.10	.337E-08	.615E-08	.511E-08
15.38	.449E-08	.720E-08	.672E-08
15.92	.684E-08	.931E-08	.101E-07
16.78	.111E-07	.129E-07	.158E-07
18.10	.187E-07	.193E-07	.257E-07
19.92	.312E-07	.297E-07	.412E-07
22.36	.514E-07	.471E-07	.651E-07
25.48	.802E-07	.752E-07	.101E-06
29.38	.123E-06	.120E-06	.156E-06
34.16	.185E-06	.191E-06	.238E-06
39.88	.274E-06	.302E-06	.360E-06
46.62	.403E-06	.477E-06	.537E-06
54.50	.598E-06	.738E-06	.796E-06
63.58	.878E-06	.110E-05	.117E-05
67.02	.100E-05	.125E-05	.133E-05

**TABLE - 13:** Comparison of (da/dN) vs.  $\Delta K$  values for Mn-Mo cast steel. Equation 9 (Kujawski-Ellyin), best fit, and the proposed Equation 64 (Continued).  
for:  $R = 0.5$

$\Delta K$ [MPa $\sqrt{m}$ ]	(da/dN) <sub>EQ. 11</sub> [m/cycles]	(da/dN) <sub>Best Fit</sub> [m/cycles]	(da/dN) <sub>EQ. 64</sub> [m/cycles]
12.68	.506E-08	.557E-08	.818E-08
12.76	.537E-08	.584E-08	.864E-08
13.04	.648E-08	.680E-08	.103E-07
13.56	.868E-08	.874E-08	.135E-07
14.42	.127E-07	.124E-07	.191E-07
15.72	.196E-07	.189E-07	.283E-07
17.54	.308E-07	.301E-07	.427E-07
19.94	.482E-07	.487E-07	.643E-07
23.02	.750E-07	.791E-07	.970E-07
26.88	.116E-06	.128E-06	.147E-06
31.60	.176E-06	.205E-06	.221E-06
37.26	.265E-06	.322E-06	.332E-06
43.94	.392E-06	.500E-06	.496E-06
51.72	.573E-06	.762E-06	.735E-06
60.70	.834E-06	.114E-05	.108E-05
62.68	.900E-06	.124E-05	.117E-05

**TABLE - 14:** Comparison of  $(da/dN)$  vs.  $\Delta K$  values for 0050A cast steel. Equation 9 (Kujawski-Ellyin), best fit, and the proposed Equation 64.

for:  $R = 0$

$\Delta K$ [MPa $\sqrt{m}$ ]	$(da/dN)_{EQ. 11}$ [m/cycles]	$(da/dN)_{Best Fit}$ [m/cycles]	$(da/dN)_{EQ. 64}$ [m/cycles]
15.46	.505E-06	.996E-08	.778E-08
15.54	.531E-06	.103E-07	.817E-08
15.80	.617E-08	.114E-07	.948E-08
16.32	.805E-08	.138E-07	.123E-07
17.18	.116E-07	.182E-07	.177E-07
18.46	.179E-07	.260E-07	.272E-07
20.24	.288E-07	.394E-07	.434E-07
22.62	.474E-07	.621E-07	.708E-07
25.68	.787E-07	.101E-06	.116E-06
29.48	.130E-06	.166E-06	.191E-06
34.12	.215E-06	.279E-06	.312E-06
39.70	.351E-06	.476E-06	.508E-06
46.30	.569E-06	.823E-06	.818E-06
53.98	.911E-06	.144E-05	.130E-05
55.68	.100E-05	.162E-05	.143E-05



**TABLE - 14:** Comparison of (da/dN) vs.  $\Delta K$  values for 0050A cast steel. Equation 9 (Kujawski-Ellyin), best fit, and the proposed Equation 64 (Continued).

for:  $R = 0.5$

$\Delta K$ [MPa $\sqrt{m}$ ]	(da/dN) <sub>EQ. 11</sub> [m/cycles]	(da/dN) <sub>Best Fit</sub> [m/cycles]	(da/dN) <sub>EQ. 64</sub> [m/cycles]
12.74	.503E-08	.152E-07	.772E-08
12.82	.526E-08	.158E-07	.806E-08
13.08	.605E-08	.176E-07	.922E-08
13.60	.777E-08	.212E-07	.117E-07
14.46	.110E-07	.265E-07	.164E-07
15.72	.163E-07	.337E-07	.245E-07
17.50	.257E-07	.434E-07	.384E-07
19.86	.414E-07	.573E-07	.618E-07
22.90	.681E-07	.817E-07	.101E-06
26.68	.113E-06	.131E-06	.166E-06
31.32	.187E-06	.240E-07	.273E-06
32.04	.200E-06	.262E-07	.293E-06

**TABLE - 15:** Comparison of  $(da/dN)$  vs.  $\Delta K$  values for 7075-T6 aluminum. Best fit through the experimental data, and the proposed Equation 64.  
for:  $R = 0.0$

$\Delta K$ [MPa $\sqrt{m}$ ]	$(da/dN)_{\text{Best Fit}}$ [m/cycles]	$(da/dN)_{\text{EQ. 64}}$ [m/cycles]
4.78	.705E-07	.492E-07
4.83	.792E-07	.532E-07
4.99	.104E-06	.661E-07
5.31	.145E-06	.955E-07
5.82	.200E-06	.157E-06
6.60	.272E-06	.283E-06
7.58	.385E-06	.539E-06
9.11	.605E-06	.105E-05
10.94	.104E-05	.207E-05
13.24	.184E-05	.406E-05
16.05	.336E-05	.787E-05
19.41	.664E-05	.150E-04
23.39	.148E-04	.280E-04
28.02	.374E-04	.512E-04
33.37	.116E-03	.914E-04
34.30	.142E-03	.100E-03

**TABLE - 15:** Comparison of  $(da/dN)$  vs.  $\Delta K$  values for 7075-T6 aluminum. Best fit through the experimental data, and the proposed Equation 64 (Continued).  
for:  $R = 0.2$

$\Delta K$ [MPa $\sqrt{m}$ ]	$(da/dN)_{\text{Best Fit}}$ [m/cycles]	$(da/dN)_{\text{EQ. 64}}$ [m/cycles]
7.10	.421E-06	.502E-06
7.15	.416E-06	.514E-06
7.30	.407E-06	.556E-06
7.59	.425E-06	.641E-06
8.06	.522E-06	.797E-06
8.76	.768E-06	.108E-05
9.74	.120E-05	.156E-05
11.05	.179E-05	.241E-05
12.73	.267E-05	.389E-05
14.82	.450E-05	.648E-05
17.39	.891E-05	.110E-04
20.46	.186E-04	.189E-04
24.09	.415E-04	.323E-04
28.32	.123E-03	.550E-04

**TABLE - 15:** Comparison of  $(da/dN)$  vs.  $\Delta K$  values for 7075-T6 aluminum. Best fit through the experimental data, and the proposed Equation 64 (Continued).  
for:  $R = 0.33$

$\Delta K$ [MPa $\sqrt{m}$ ]	$(da/dN)_{\text{Best Fit}}$ [m/cycles]	$(da/dN)_{\text{EQ. 64}}$ [m/cycles]
5.57	.363E-06	.215E-06
5.62	.372E-06	.224E-06
5.78	.396E-06	.249E-06
6.07	.435E-06	.304E-06
6.57	.503E-06	.410E-06
7.31	.646E-06	.608E-06
8.33	.960E-06	.972E-06
9.70	.153E-05	.164E-05
11.46	.244E-05	.289E-05
13.64	.420E-05	.517E-05
16.33	.847E-05	.934E-05
19.53	.230E-04	.168E-04
23.33	.139E-03	.300E-04
27.75	.113E-02	.529E-04

**TABLE - 15:** Comparison of  $(da/dN)$  vs.  $\Delta K$  values for 7075-T6 aluminum. Best fit through the experimental data, and the proposed Equation 64 (Continued).

for:  $R = 0.5$

$\Delta K$ [MPa $\sqrt{m}$ ]	$(da/dN)_{\text{Best Fit}}$ [m/cycles]	$(da/dN)_{\text{EQ. 64}}$ [m/cycles]
4.38	.152E-06	.101E-06
4.43	.158E-06	.106E-06
4.59	.174E-06	.124E-06
4.90	.213E-06	.164E-06
5.41	.290E-06	.242E-06
6.16	.449E-06	.396E-06
7.22	.782E-06	.697E-06
8.63	.148E-05	.128E-05
10.44	.299E-05	.240E-05
12.70	.655E-05	.455E-05
15.45	.160E-04	.858E-05
18.76	.435E-04	.160E-04

**TABLE - 15:** Comparison of  $(da/dN)$  vs.  $\Delta K$  values for 7075-T6 aluminum. Best fit through the experimental data, and the proposed Equation 64 (Continued).

for:  $R = 0.7$

$\Delta K$ [MPa $\sqrt{m}$ ]	$(da/dN)_{\text{Best Fit}}$ [m/cycles]	$(da/dN)_{\text{EQ. 64}}$ [m/cycles]
3.05	.689E-07	.502E-07
3.11	.734E-07	.546E-07
3.27	.866E-07	.687E-07
3.58	.114E-06	.101E-06
4.10	.172E-06	.169E-06
4.88	.316E-06	.310E-06
5.96	.705E-06	.595E-06
7.40	.183E-05	.117E-05
9.24	.551E-05	.232E-05

**TABLE - 15:** Comparison of  $(da/dN)$  vs.  $\Delta K$  values for 7075-T6 aluminum. Best fit through the experimental data, and the proposed Equation 64 (Continued).

for:  $R = 0.8$

$\Delta K$ [MPa $\sqrt{m}$ ]	$(da/dN)_{\text{Best Fit}}$ [m/cycles]	$(da/dN)_{\text{EQ. 64}}$ [m/cycles]
2.30	.348E-07	.502E-07
2.35	.403E-07	.551E-07
2.51	.549E-07	.711E-07
2.83	.792E-07	.108E-06
3.35	.129E-06	.187E-06
4.13	.283E-06	.353E-06
5.21	.843E-06	.691E-06
6.66	.334E-05	.138E-05

**TABLE - 16:** Comparison of  $(da/dN)$  vs.  $\Delta K$  values for 2024-T3 aluminum. Best fit through the experimental data, and the proposed Equation 64.  
for:  $R = 0.0$

$\Delta K$ [MPa $\sqrt{m}$ ]	$(da/dN)_{\text{Best Fit}}$ [m/cycles]	$(da/dN)_{\text{EQ. 64}}$ [m/cycles]
3.63	.422E-08	.506E-08
3.68	.495E-08	.563E-08
3.84	.733E-08	.748E-08
4.16	.125E-07	.118E-07
4.68	.219E-07	.213E-07
5.46	.500E-07	.411E-07
6.55	.900E-07	.819E-07
8.00	.200E-06	.165E-06
9.85	.300E-06	.332E-06
12.18	.600E-06	.665E-06
15.01	.150E-05	.132E-05
18.41	.250E-05	.257E-05
22.43	.480E-05	.492E-05
27.11	.100E-04	.924E-05
27.76	.150E-04	.100E-04



**TABLE - 16:** Comparison of  $(da/dN)$  vs.  $\Delta K$  values for 2024-T3 aluminum. Best fit through the experimental data, and the proposed Equation 64 (Continued).  
for:  $R = 0.33$

$\Delta K$ [MPa $\sqrt{m}$ ]	$(da/dN)_{\text{Best Fit}}$ [m/cycles]	$(da/dN)_{\text{EQ. 64}}$ [m/cycles]
2.84	.115E-07	.505E-08
2.89	.123E-07	.573E-08
3.05	.148E-07	.802E-08
3.38	.202E-07	.136E-07
3.90	.306E-07	.256E-07
4.68	.524E-07	.509E-07
5.78	.100E-06	.103E-06
7.23	.204E-06	.208E-06
9.10	.430E-06	.417E-06
11.43	.935E-06	.827E-06
14.29	.222E-05	.162E-05
17.70	.594E-05	.312E-05

**TABLE - 16:** Comparison of  $(da/dN)$  vs.  $\Delta K$  values for 2024-T3 aluminum. Best fit through the experimental data, and the proposed Equation 64 (Continued).  
for:  $R = 0.5$

$\Delta K$ [MPa $\sqrt{m}$ ]	$(da/dN)_{\text{Best Fit}}$ [m/cycles]	$(da/dN)_{\text{EQ. 64}}$ [m/cycles]
2.48	.100E-08	.502E-08
2.53	.400E-08	.589E-08
2.69	.713E-08	.884E-08
3.02	.116E-07	.162E-07
3.55	.261E-07	.326E-07
4.33	.539E-07	.668E-07
5.43	.120E-06	.137E-06
6.89	.252E-06	.278E-06
8.77	.528E-06	.552E-06
11.11	.144E-05	.108E-05
13.98	.444E-05	.209E-05

**TABLE - 16:** Comparison of  $(da/dN)$  vs.  $\Delta K$  values for 2024-T3 aluminum. Best fit through the experimental data, and the proposed Equation 64 (Continued).  
for:  $R = 0.7$

$\Delta K$ [MPa $\sqrt{m}$ ]	$(da/dN)_{\text{Best Fit}}$ [m/cycles]	$(da/dN)_{\text{EQ. 64}}$ [m/cycles]
2.05	.100E-08	.512E-08
2.11	.400E-08	.659E-08
2.28	.800E-08	.122E-07
2.59	.104E-07	.261E-07
3.12	.250E-07	.587E-07
3.91	.600E-07	.128E-06
5.02	.146E-06	.269E-06
6.50	.376E-06	.547E-06
8.17	.921E-06	.100E-05

**TABLE - 17:** Standard Deviation (s) of the proposed model, Equation 64, and Kujawski and Ellyin's model, Equation 9, compared with the best fit (Least-Squares) through the experimental data.

<b>Alloy &amp; R-ratio</b>	<b>s (Kujawski-Ellyin)</b>	<b>s (proposed model)</b>
<b>A533-B1</b>		
R=0.1	1.30E-09	2.00E-09
R=0.3	2.19E-09	2.18E-09
R=0.5	2.69E-09	2.59E-09
R=0.7	8.92E-10	6.66E-10
R=0.8	1.13E-09	3.57E-10
<b>4340</b>		
R=0.1	6.00E-08	2.10E-07
R=0.5	6.48E-08	4.56E-08
<b>8630</b>		
R=0.0	2.70E-08	1.90E-07
R=0.5	4.92E-08	4.51E-08
<b>C-Mn</b>		
R=0.0	5.66E-07	5.16E-07
R=0.5	6.70E-09	2.10E-08
<b>Mn-Mo</b>		
R=0.0	7.33E-08	3.77E-08
R=0.5	1.02E-07	2.06E-08
<b>0050A</b>		
R=0.0	1.68E-07	4.18E-08
R=0.5	2.23E-08	1.79E-08

**APPENDIX - A**

**FIGURES**

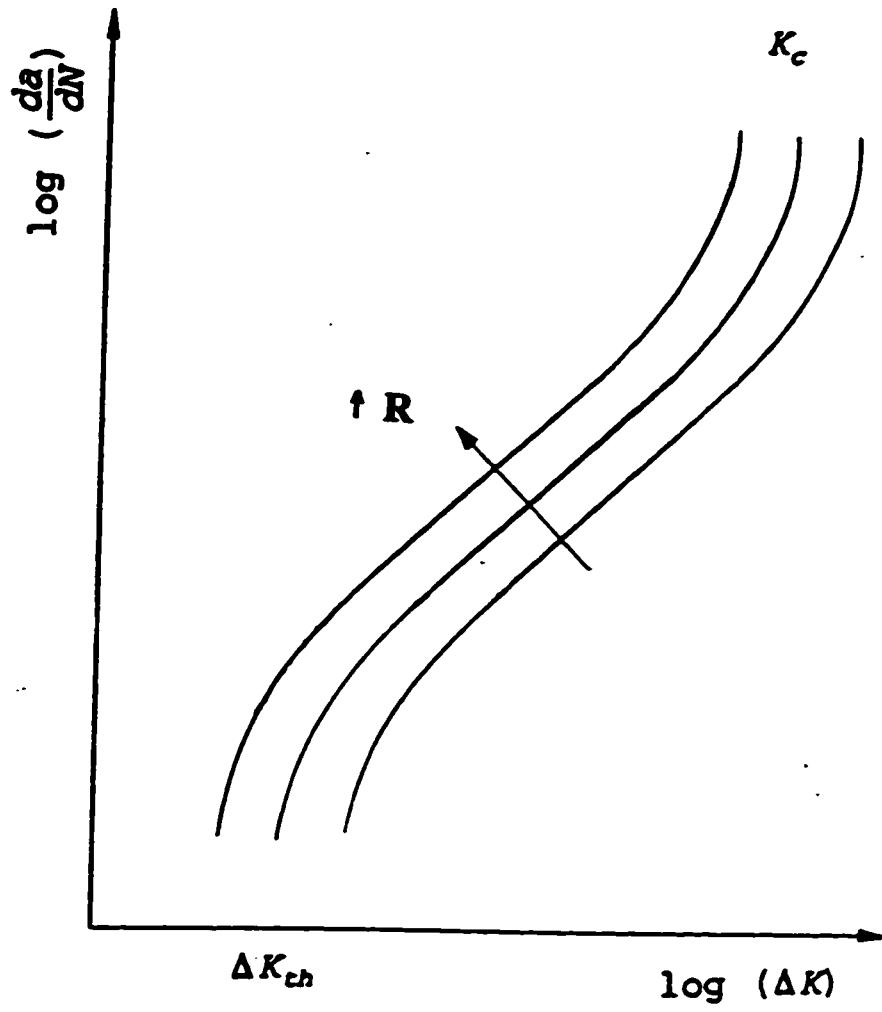


Figure 1 - Schematic illustration of the mean stress  $\sigma_m$  effect on the fatigue crack growth rate.

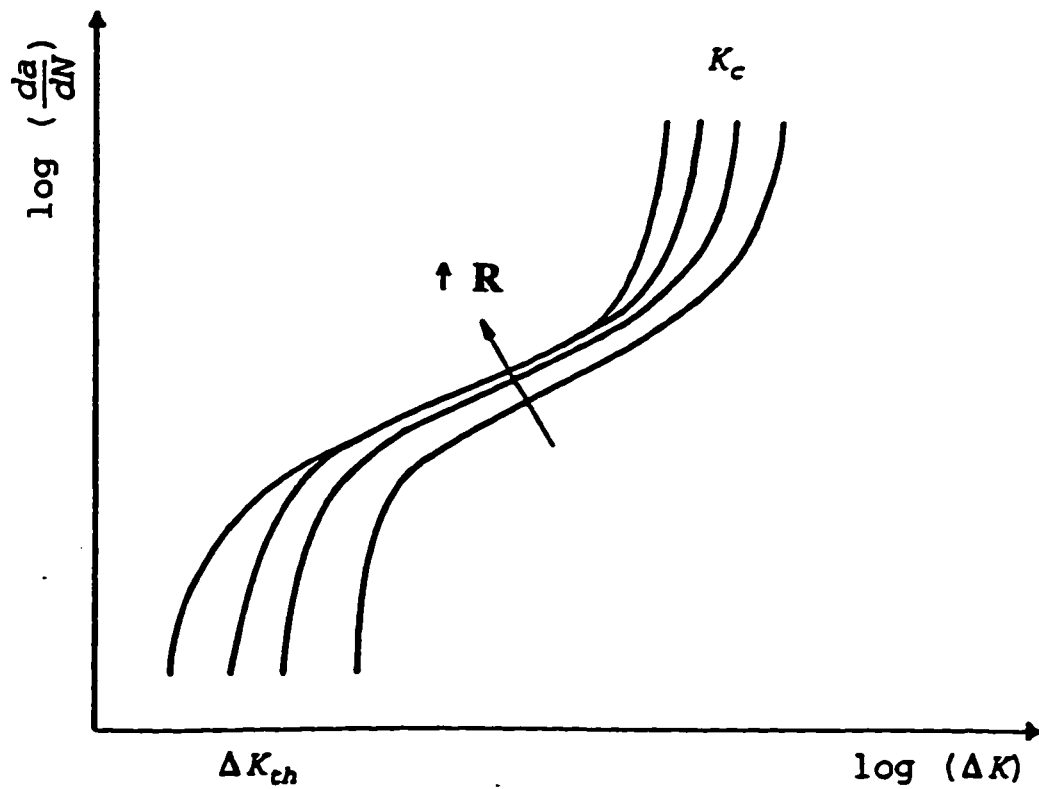


Figure 2 - Schematic illustration of the mean stress  $\sigma_m$  effect on the fatigue crack growth rate of some particular aluminum alloys.

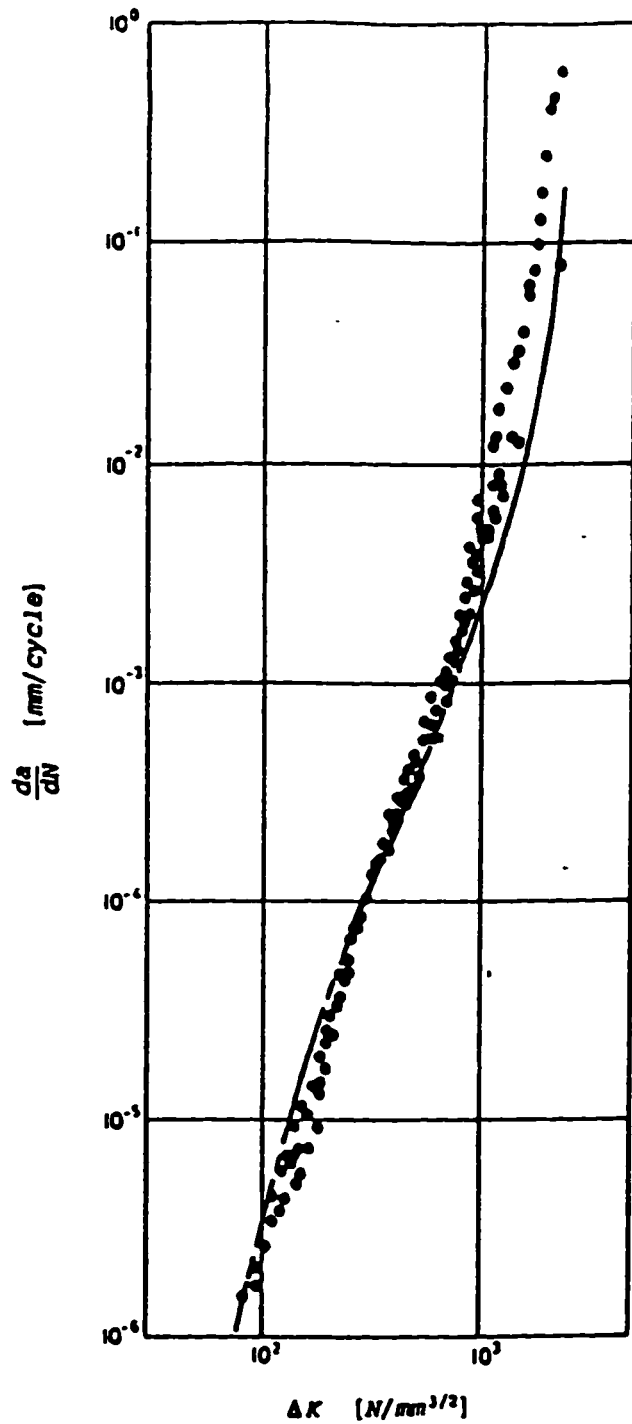


Figure 3 - Correlation of Schwalbe's crack growth model with the experimental results for AlZnMgCu0.5 aluminum alloy.



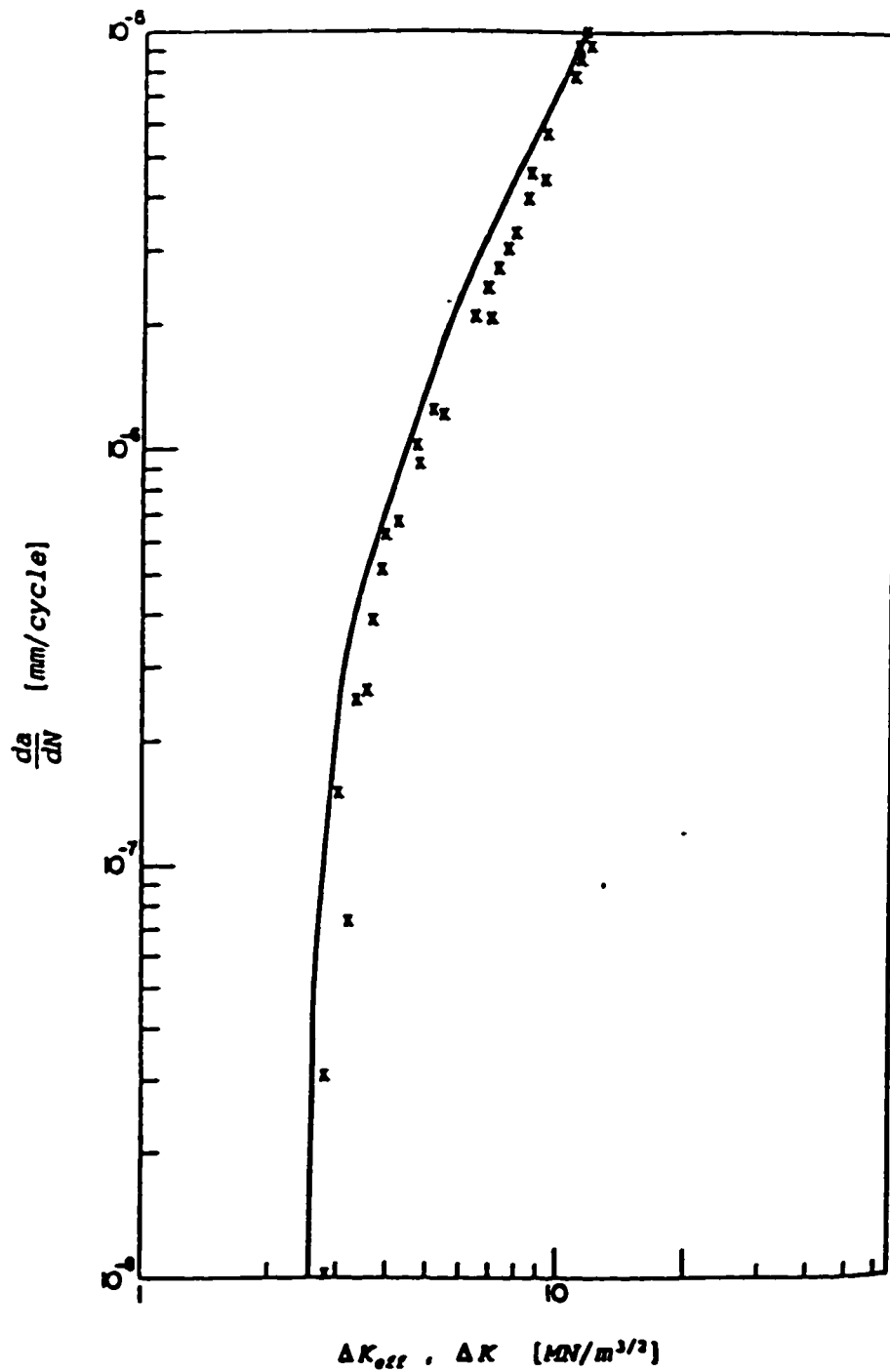


Figure 4 - Correlation of Radon's crack growth model with the experimental results for BS4360-50D steel.

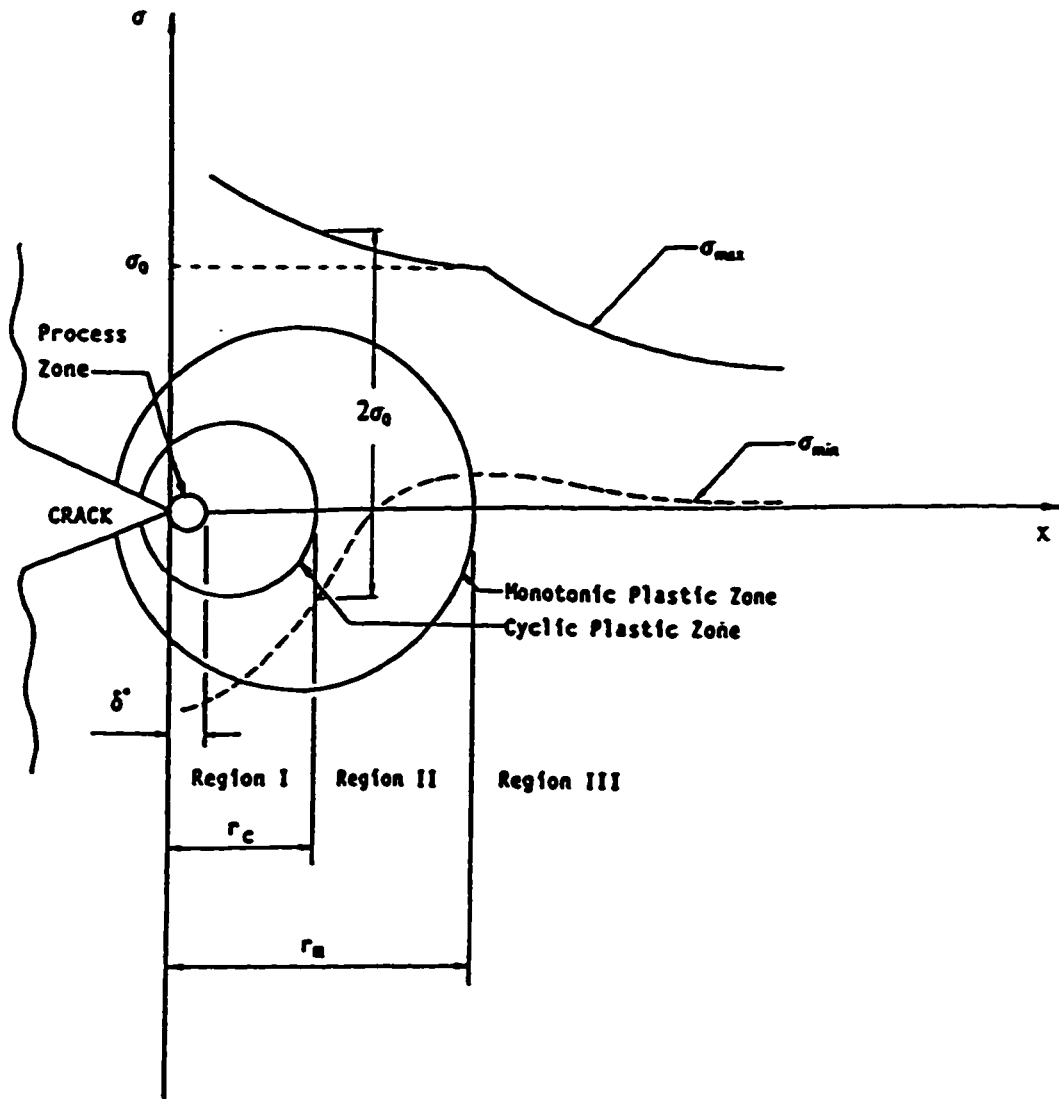


Figure 5 - Schematic plot of the cyclic stress distribution within the plastic zone.

Figure 6 - Correlation of the Kujawski-Ellyin Model with the Experimental data for A533-B1 steel

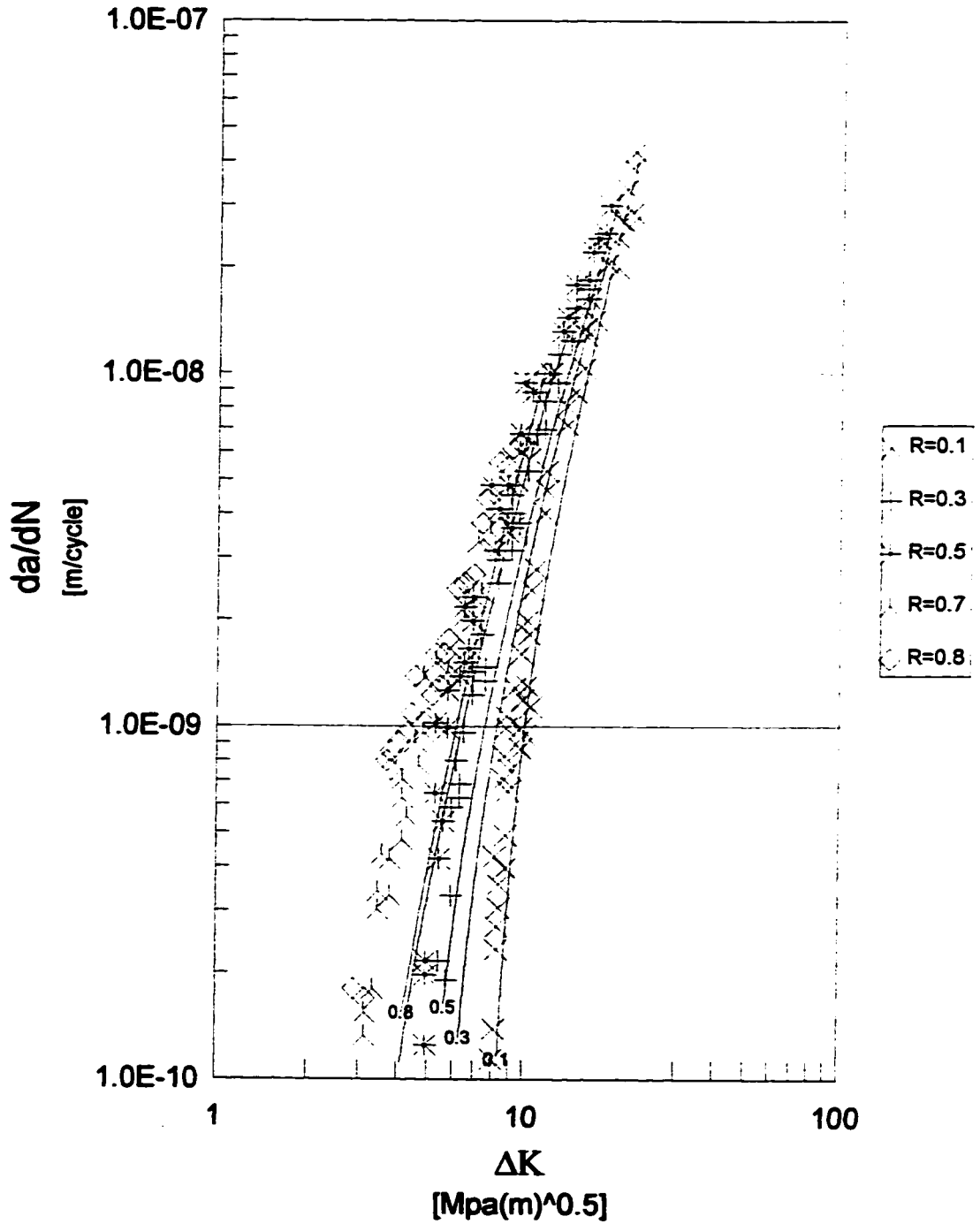


Figure 7 - Correlation of the Kujawski-Ellyin Model with the Experimental data for 4340 steel

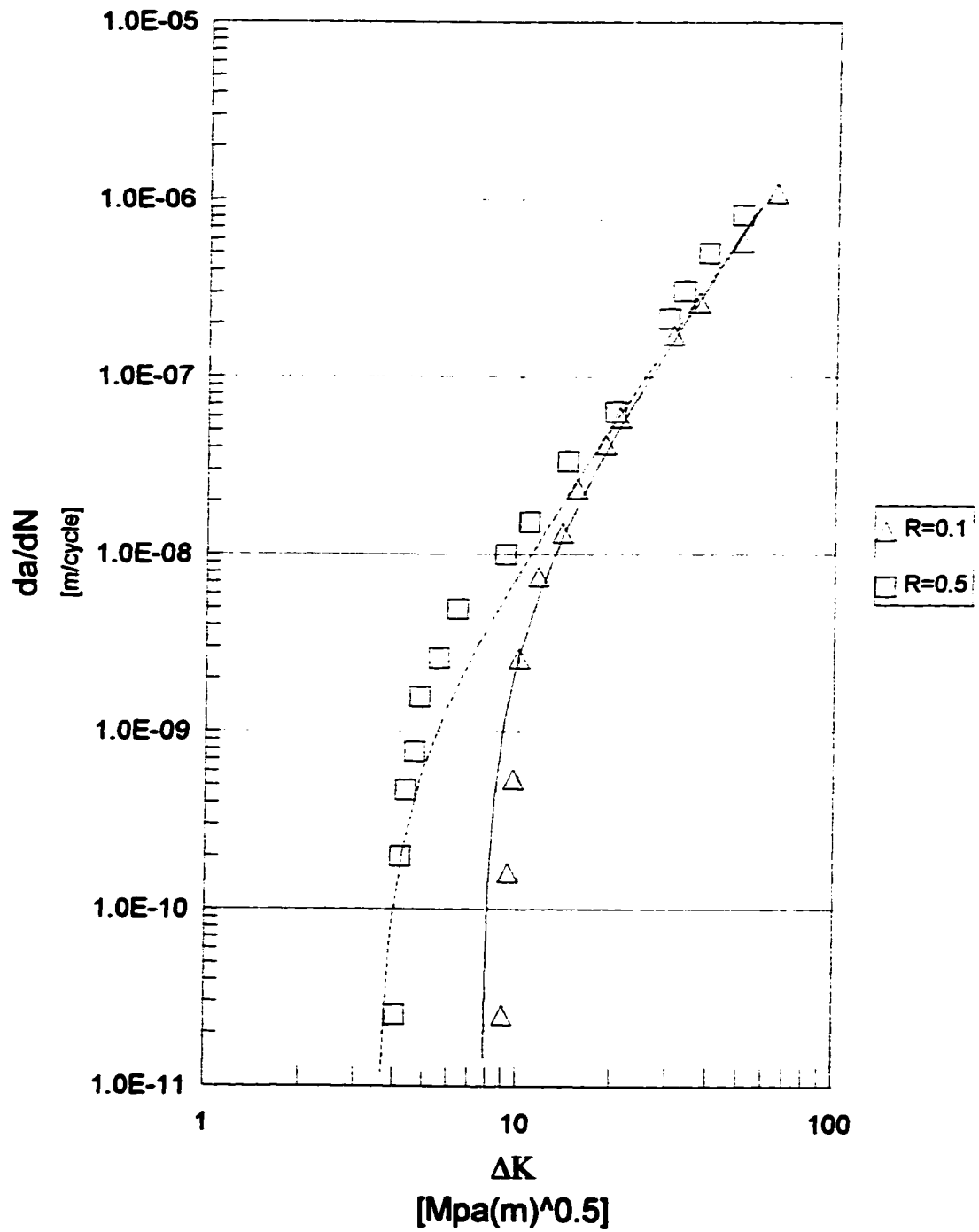


Figure 8 - Correlation of the Kujawski-Ellyin Model with the Experimental data for AISI 8630 cast steel

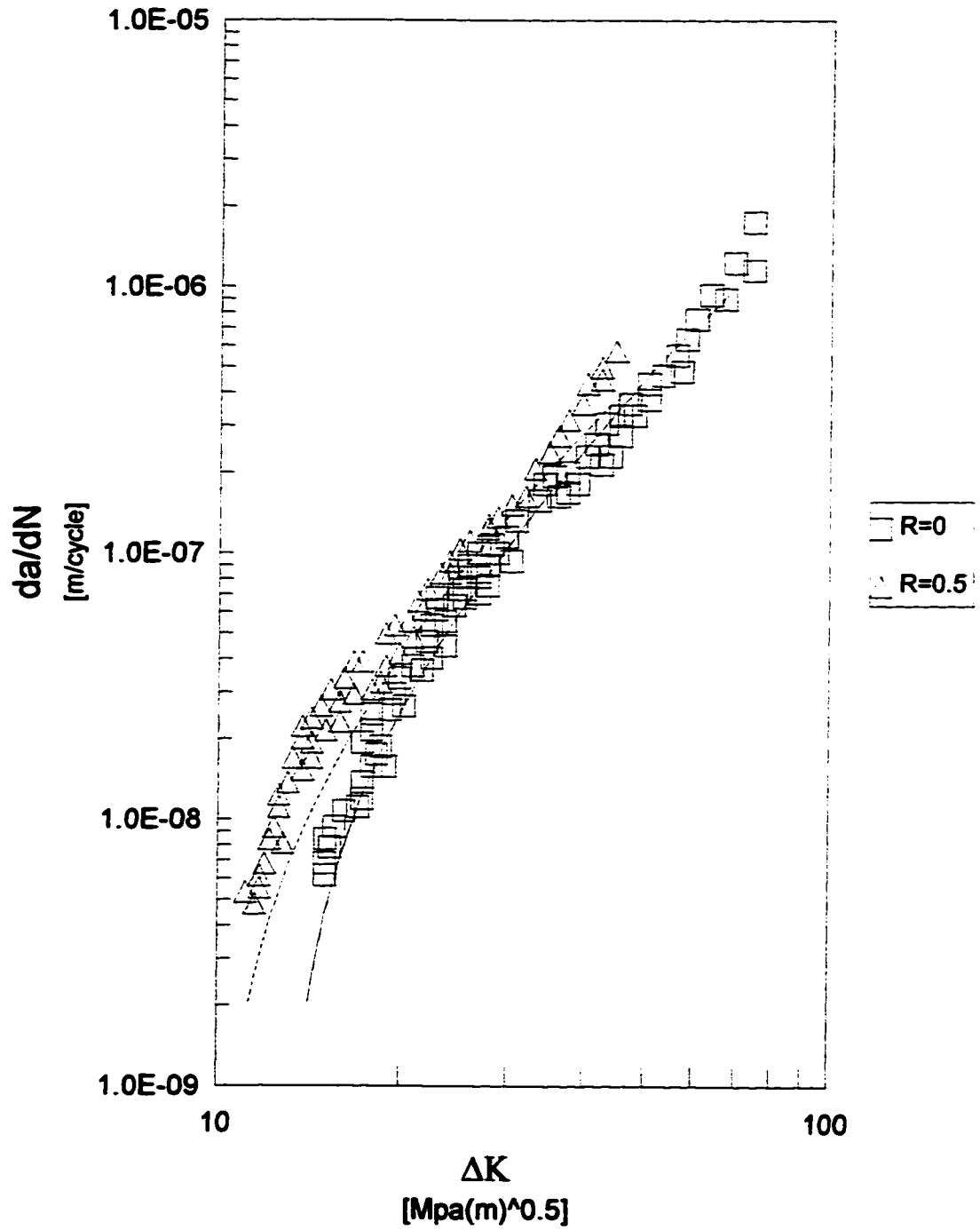


Figure 9 - Correlation of the Kujawski-Ellyin Model with the Experimental data for C-Mn cast steel

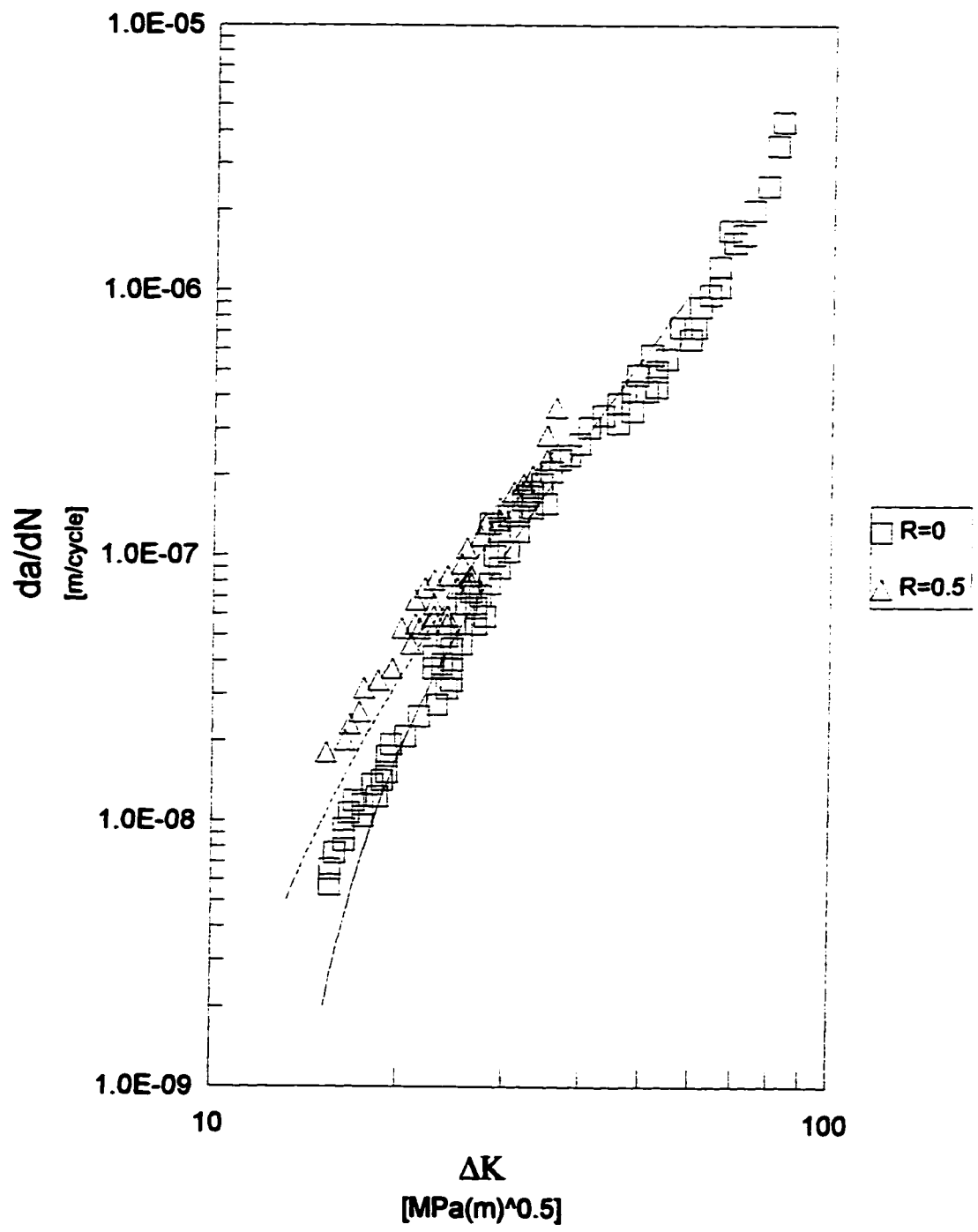


Figure 10 - Correlation of the Kujawski-Ellyin Model with the Experimental data for Mn-Mo cast steel

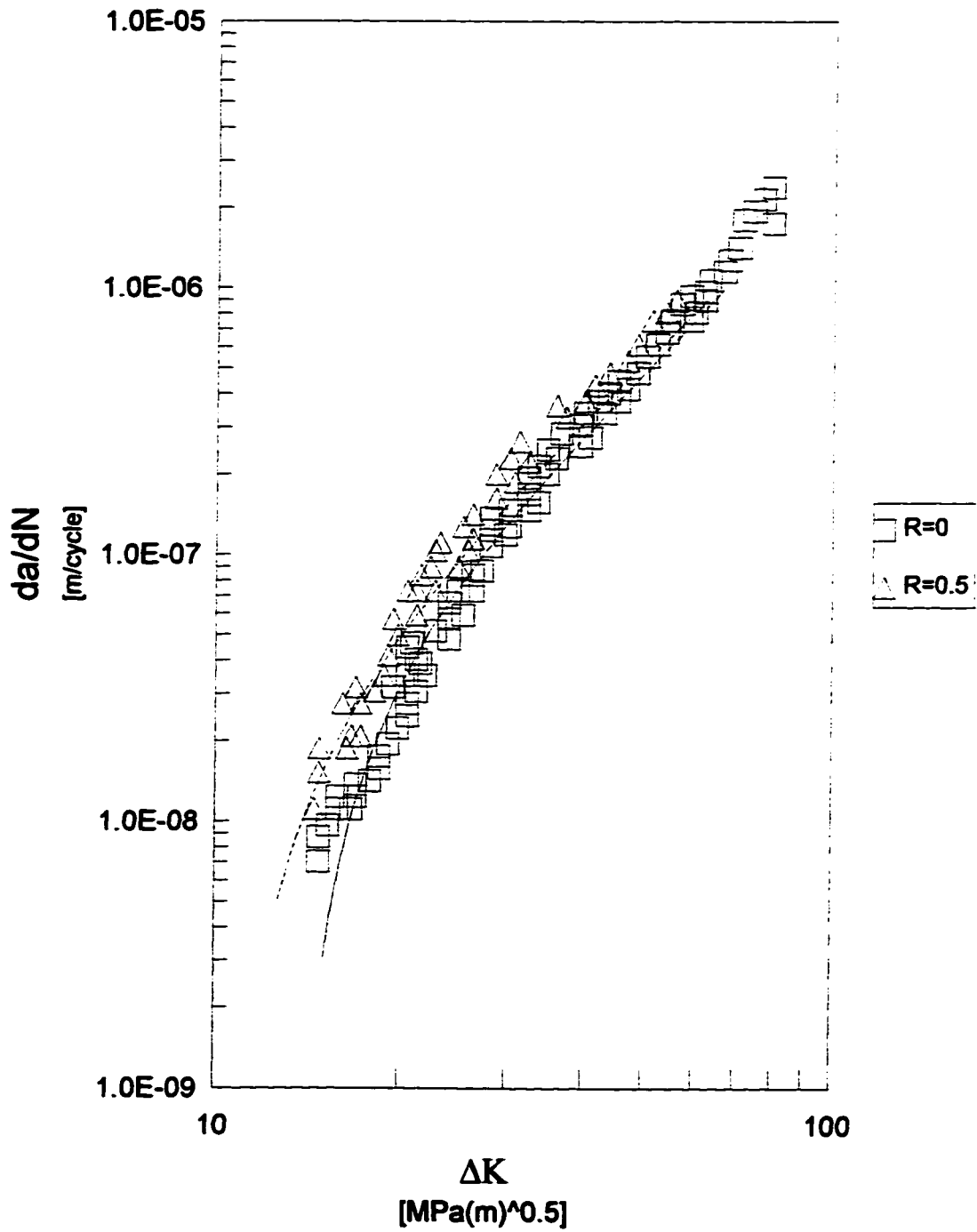


Figure 11 - Correlation of the Kujawski-Ellyin Model with the Experimental data for 0050A cast steel

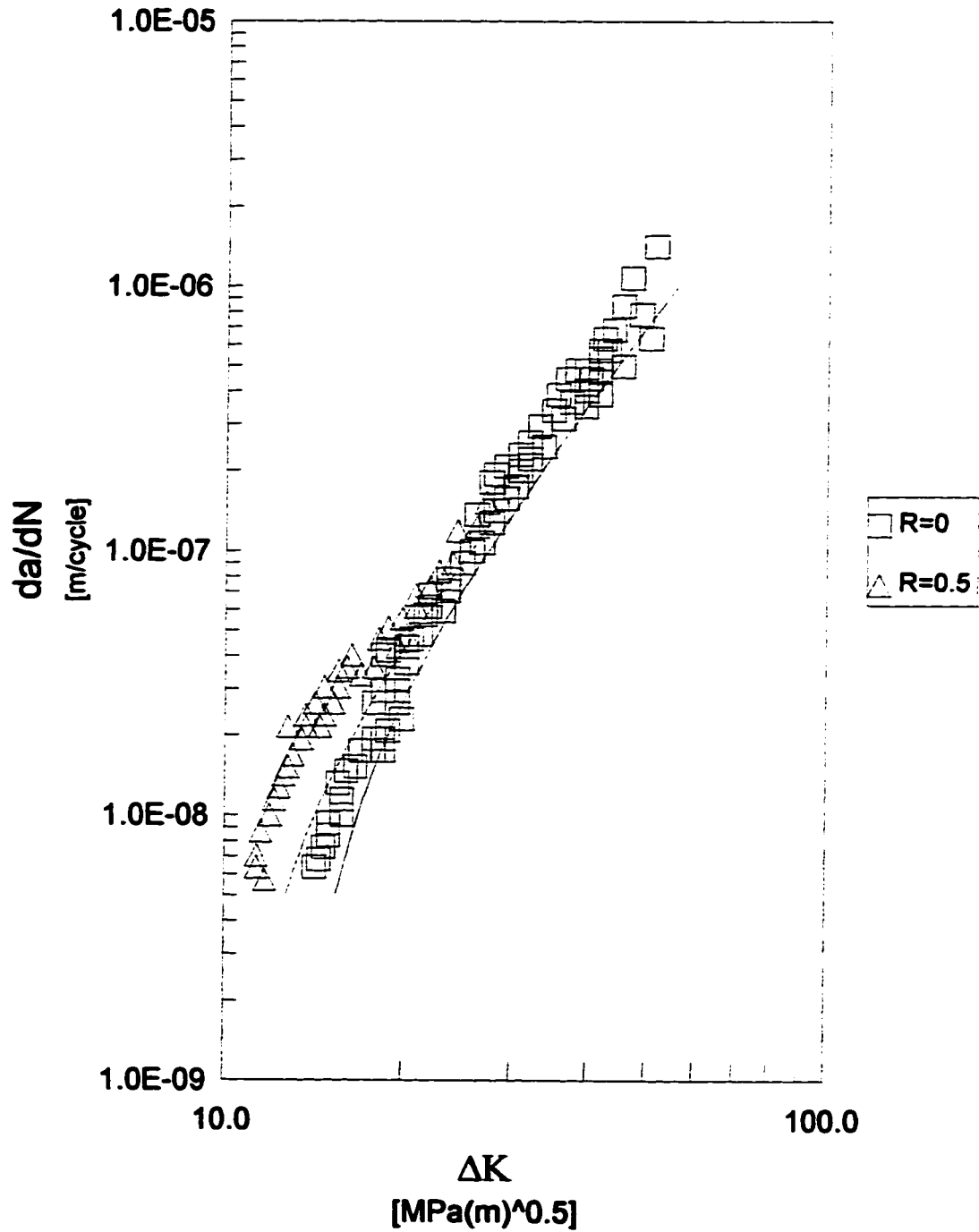
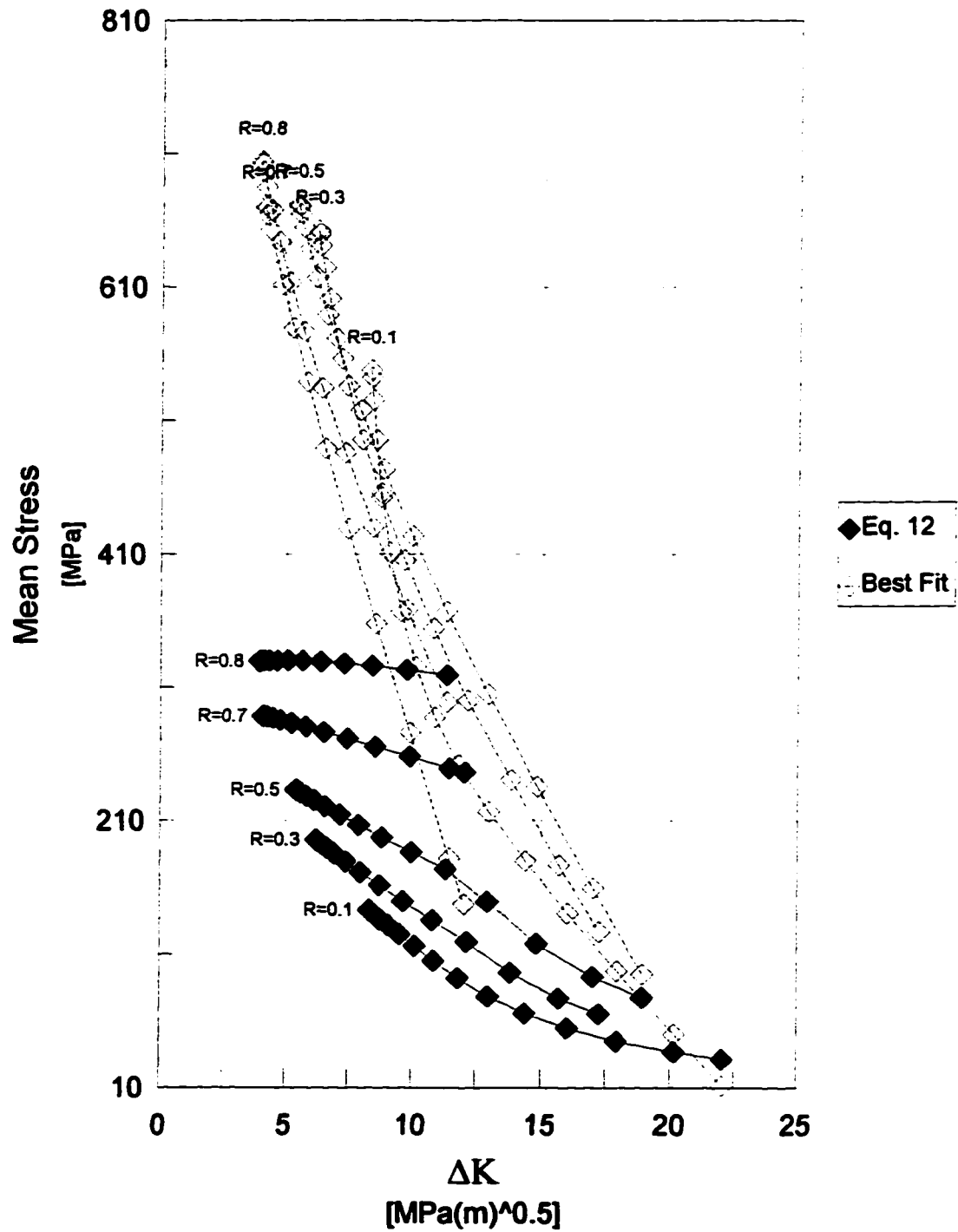




Figure 12 - Mean Stress Distribution for A533-B1 Steel



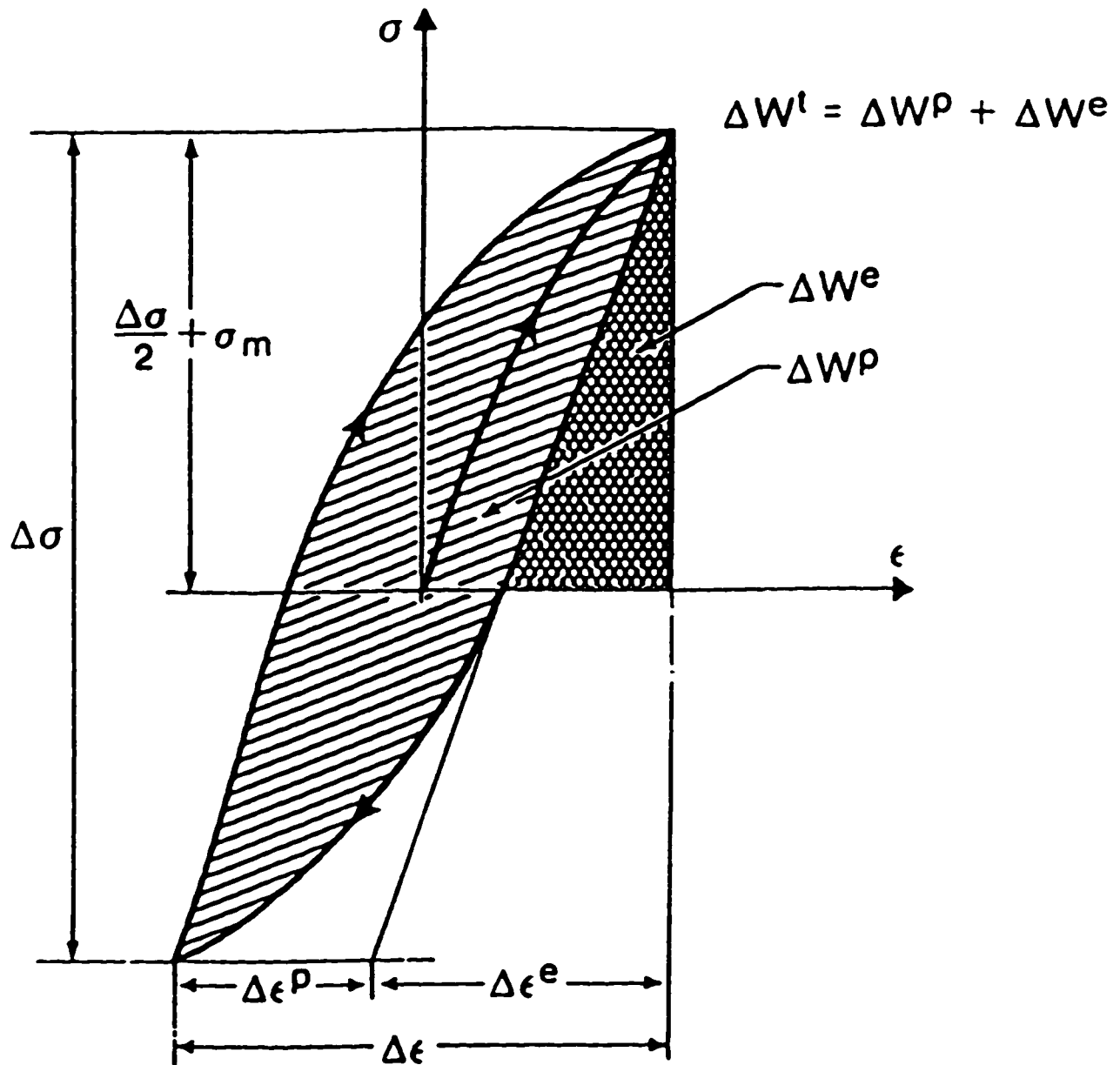


Figure 13 - Definition of the elastic, plastic and total cyclic strain energy density.

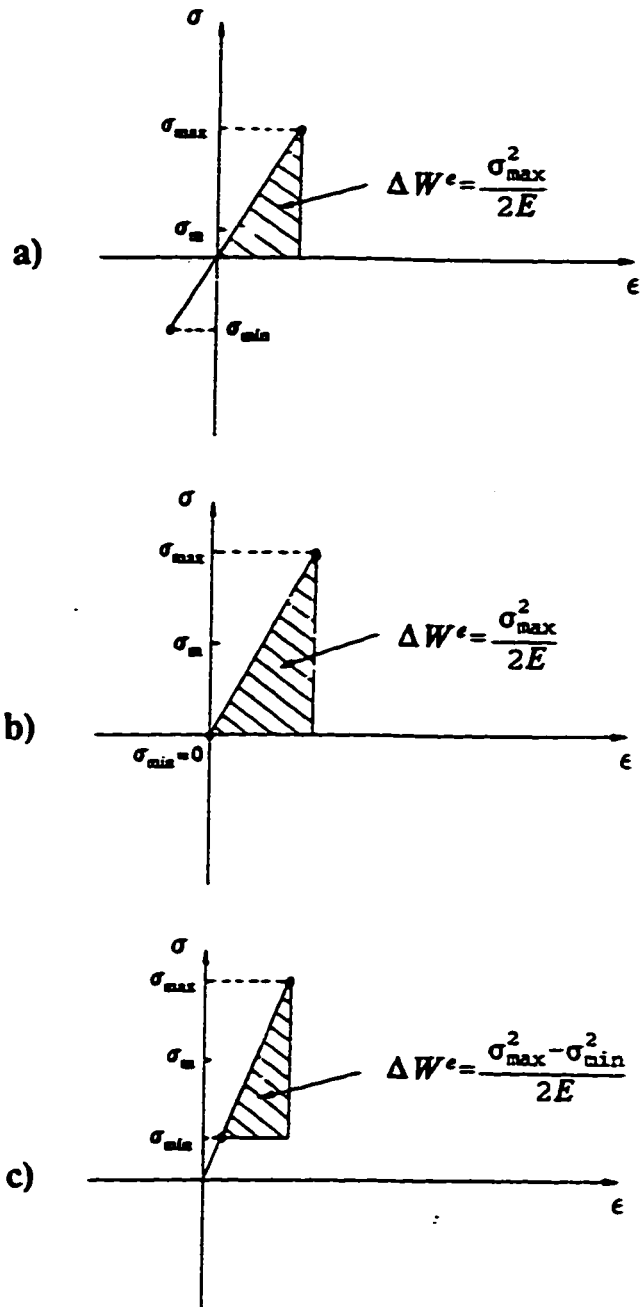


Figure 14 - Mean stress effect in the hysteresis loop.

Figure 15 - Correlation of the Proposed Model with the Experimental data for A533-B1 steel

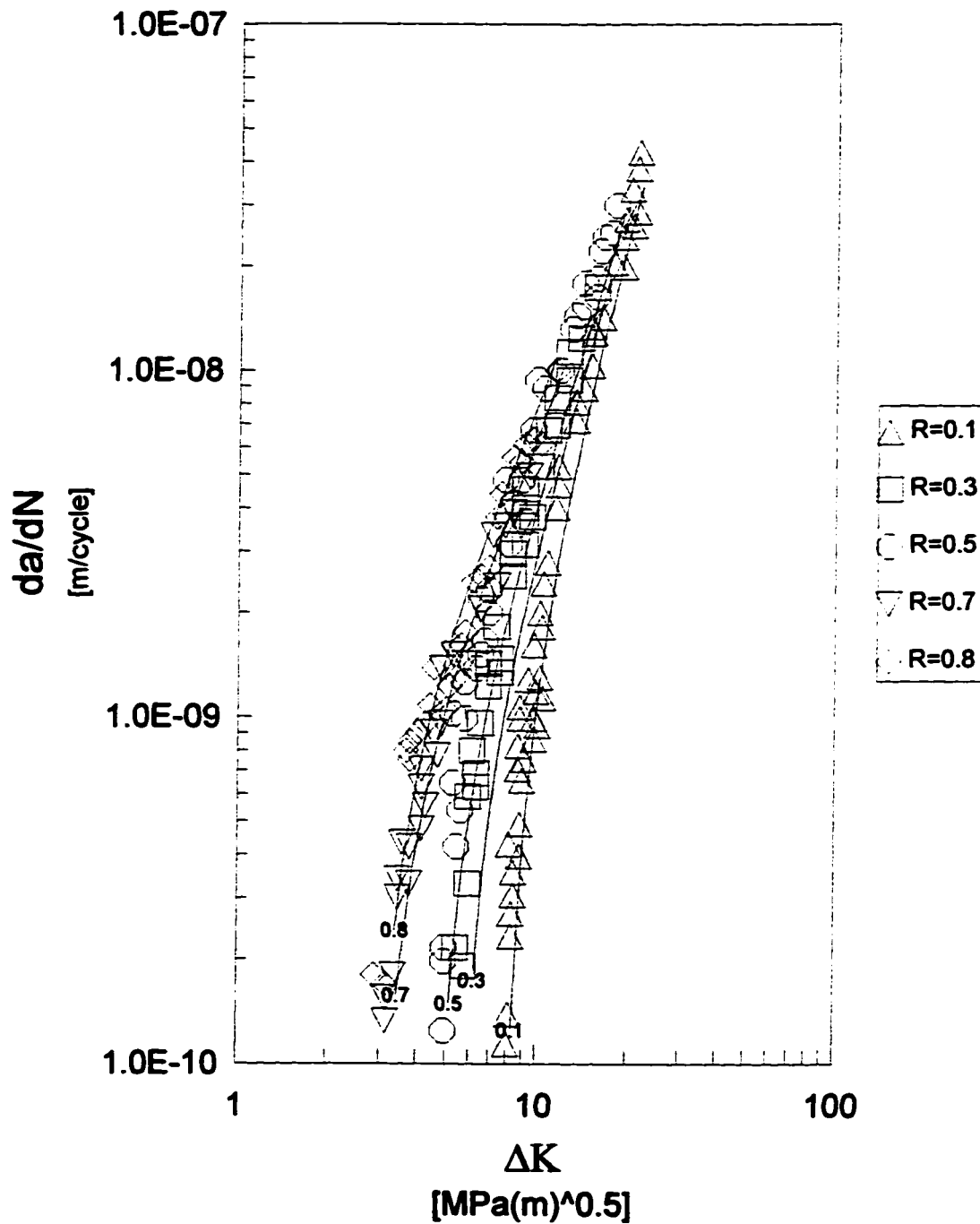


Figure 16 - Correlation of the Proposed Model with the Experimental data for 4340 steel

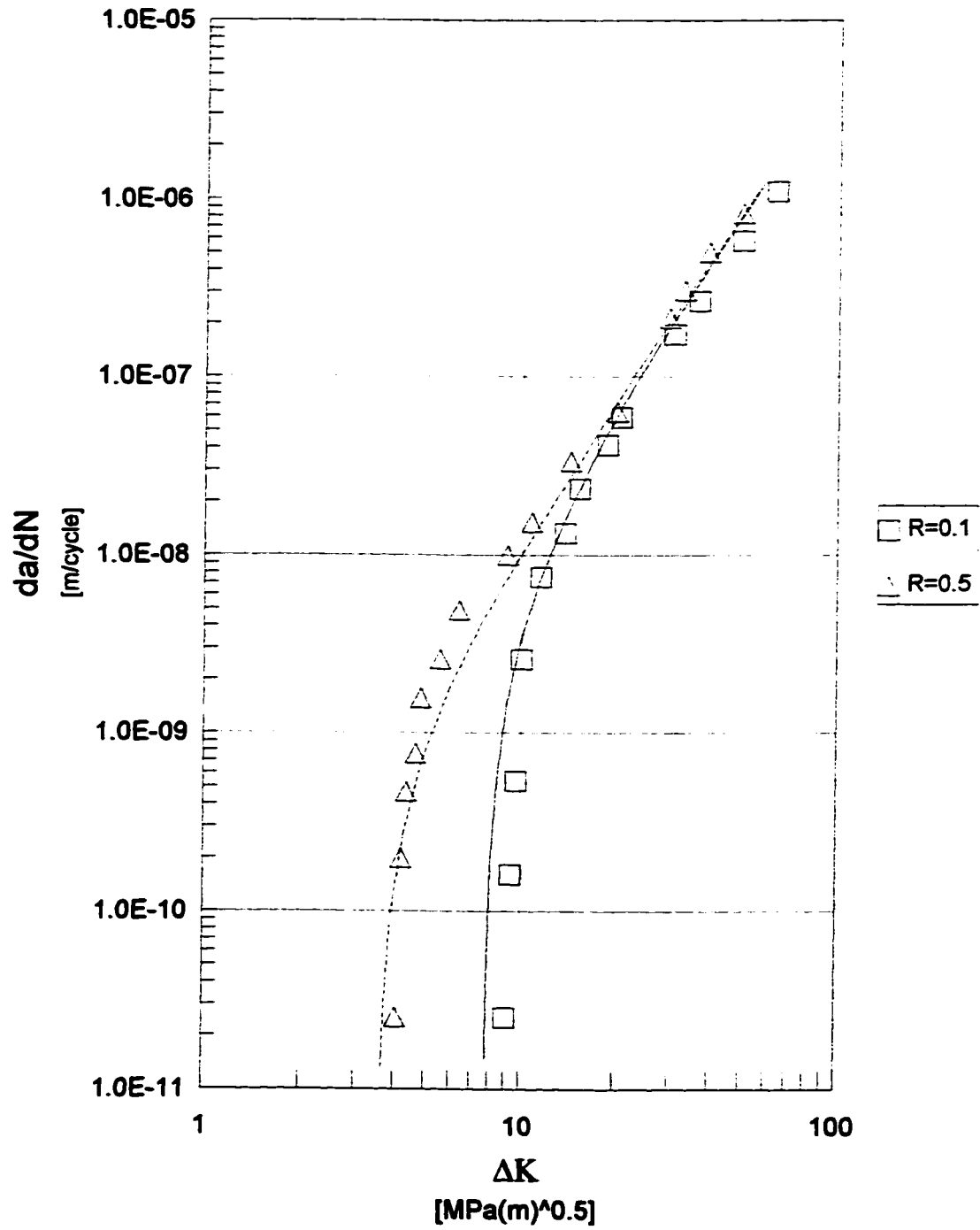


Figure 17 - Correlation of the Proposed Model with the Experimental data for 8630 cast steel

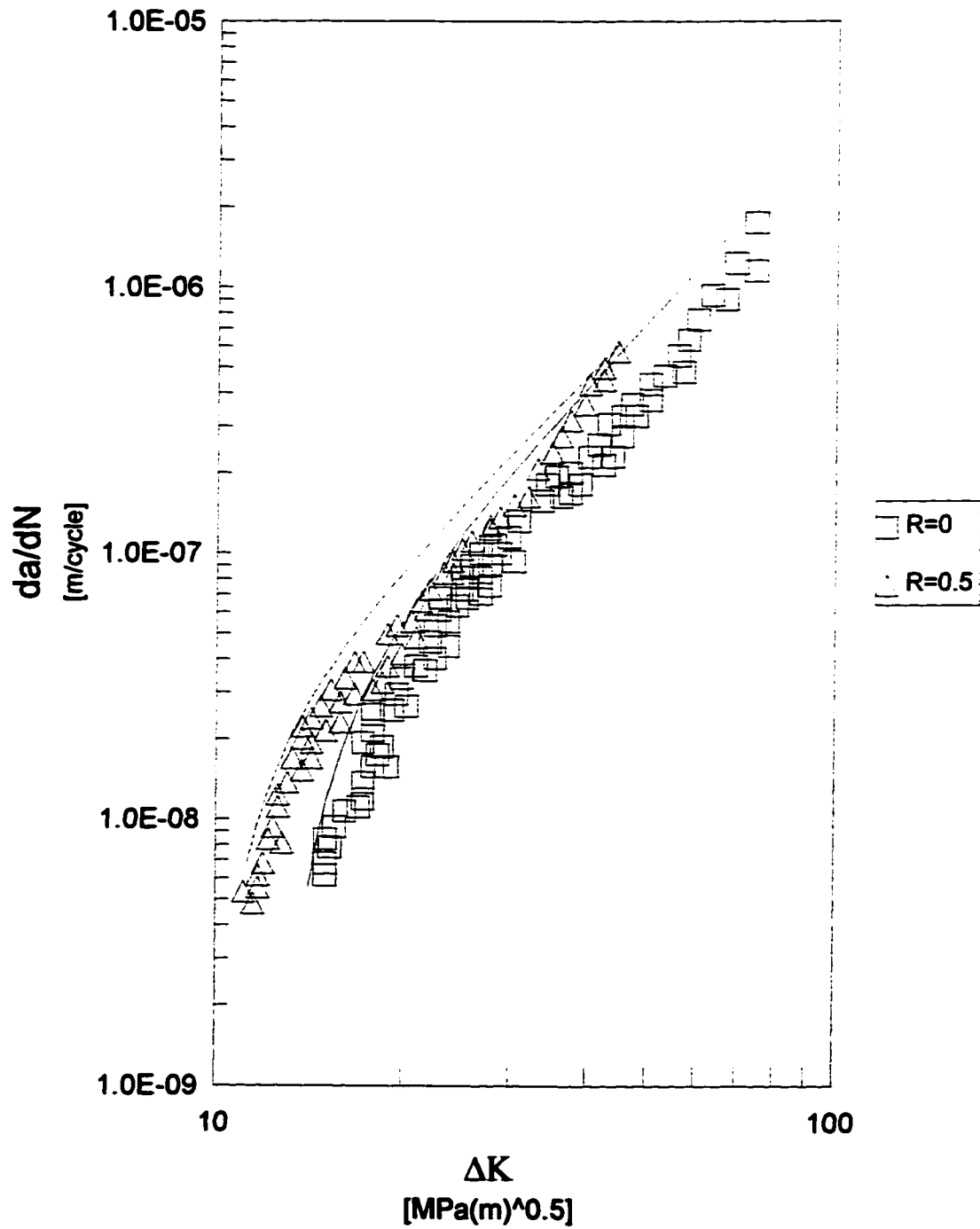


Figure 18 - Correlation of the Proposed Model with the Experimental data for C-Mn cast steel

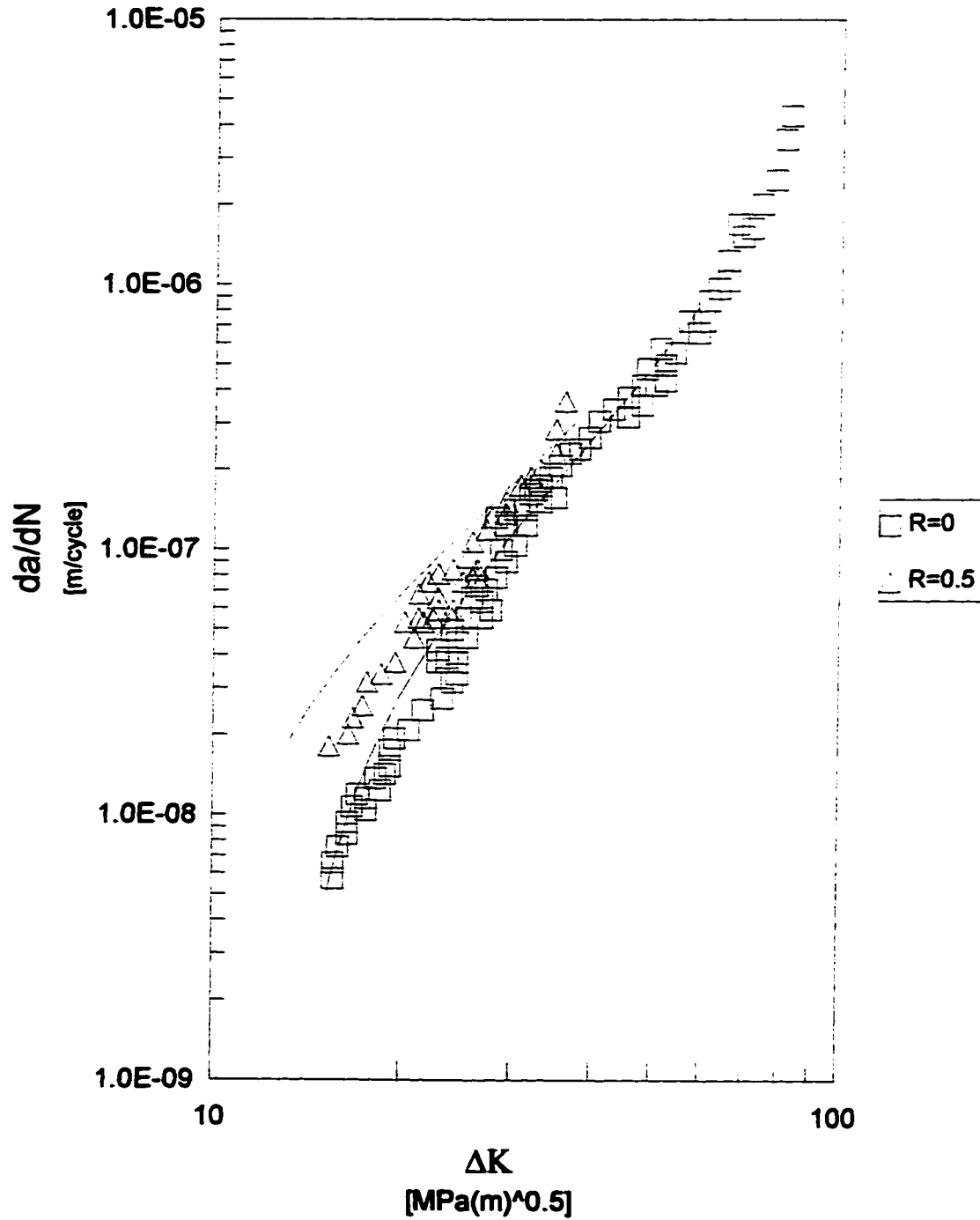


Figure 19 - Correlation of the Proposed Model with the Experimental data for Mn-Mo cast steel

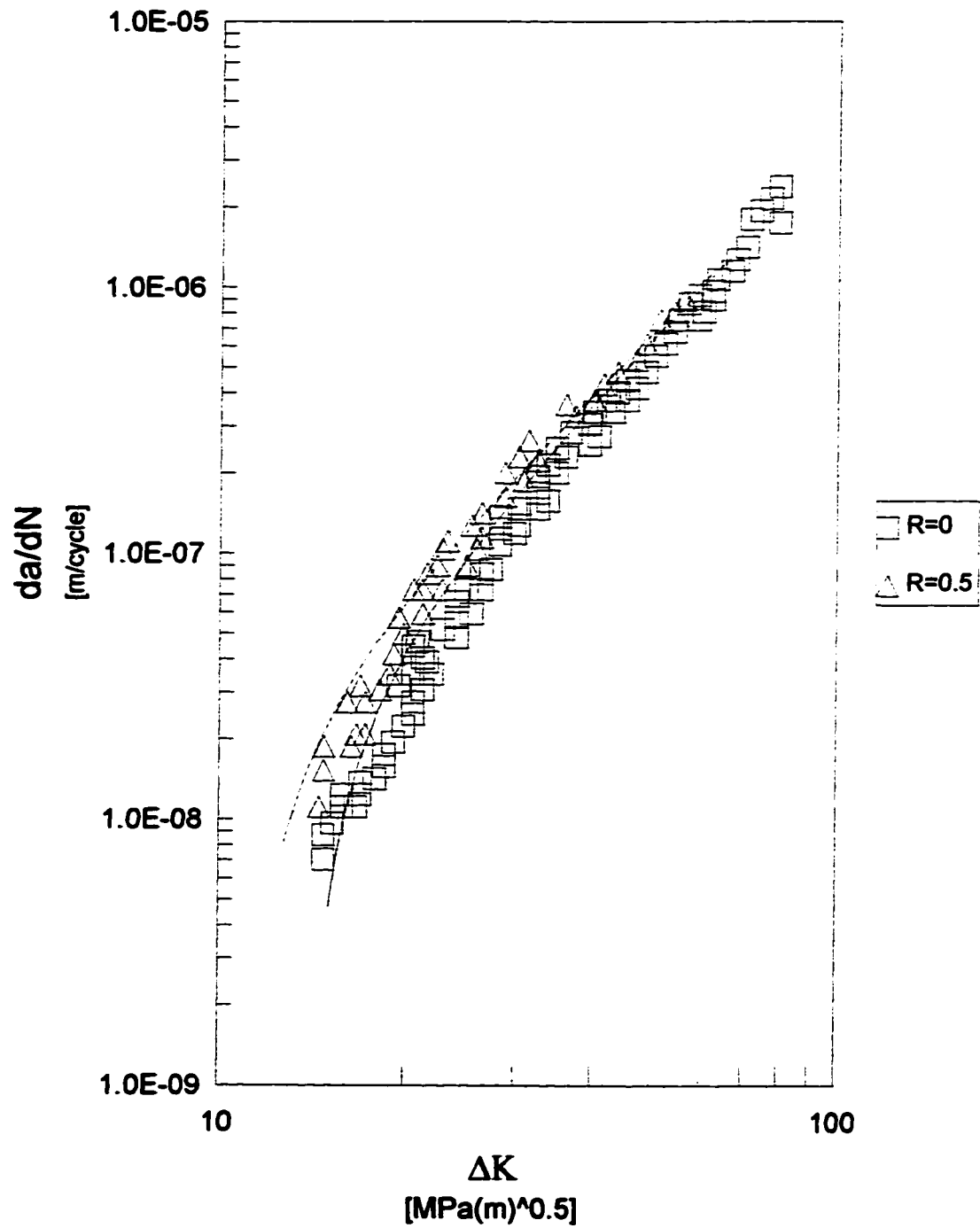




Figure 20 - Correlation of the Proposed Model with the Experimental data for 0050A cast steel

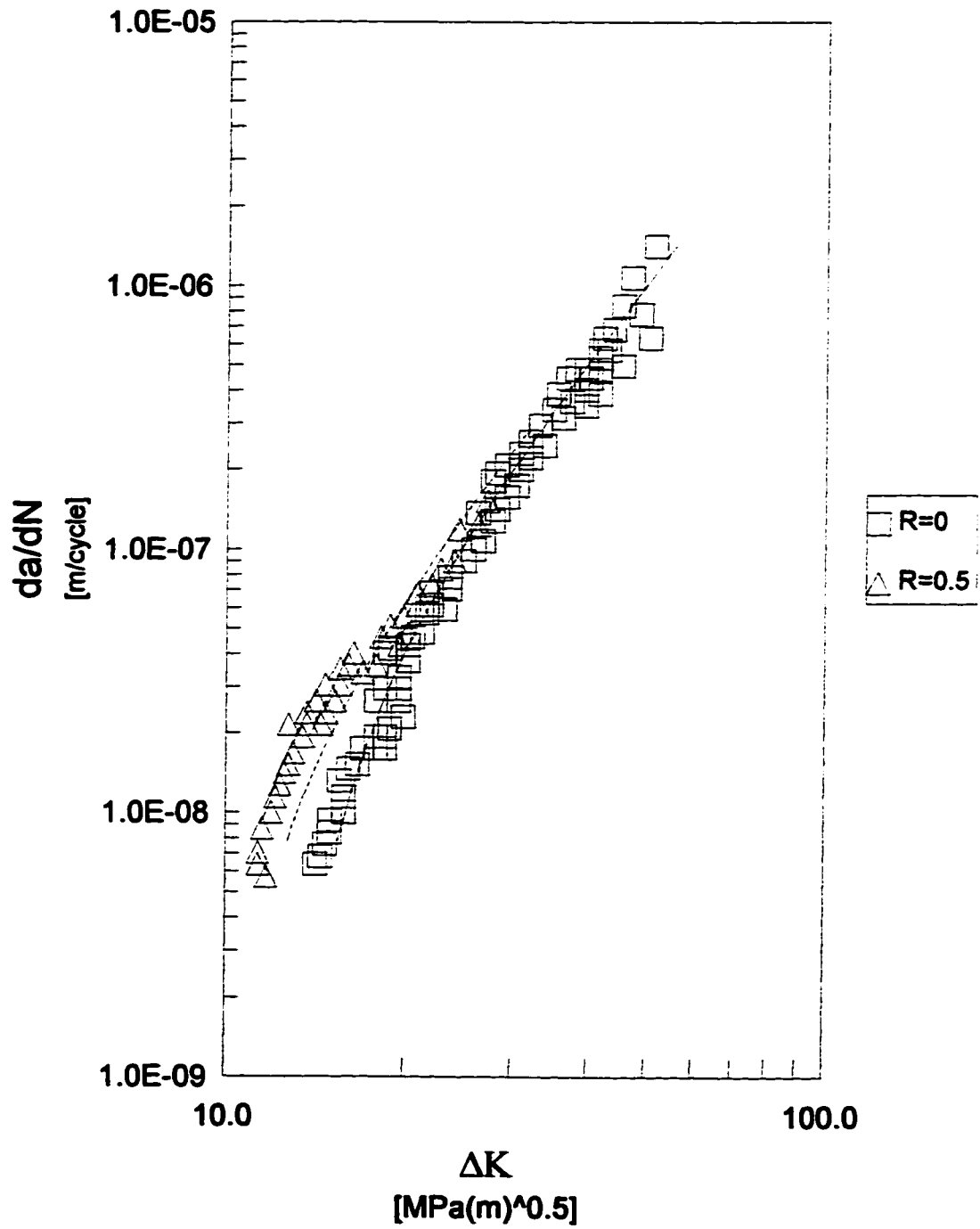


Figure 21 - Correlation of the Proposed Model with the Experimental data for Aluminum 7075-T6

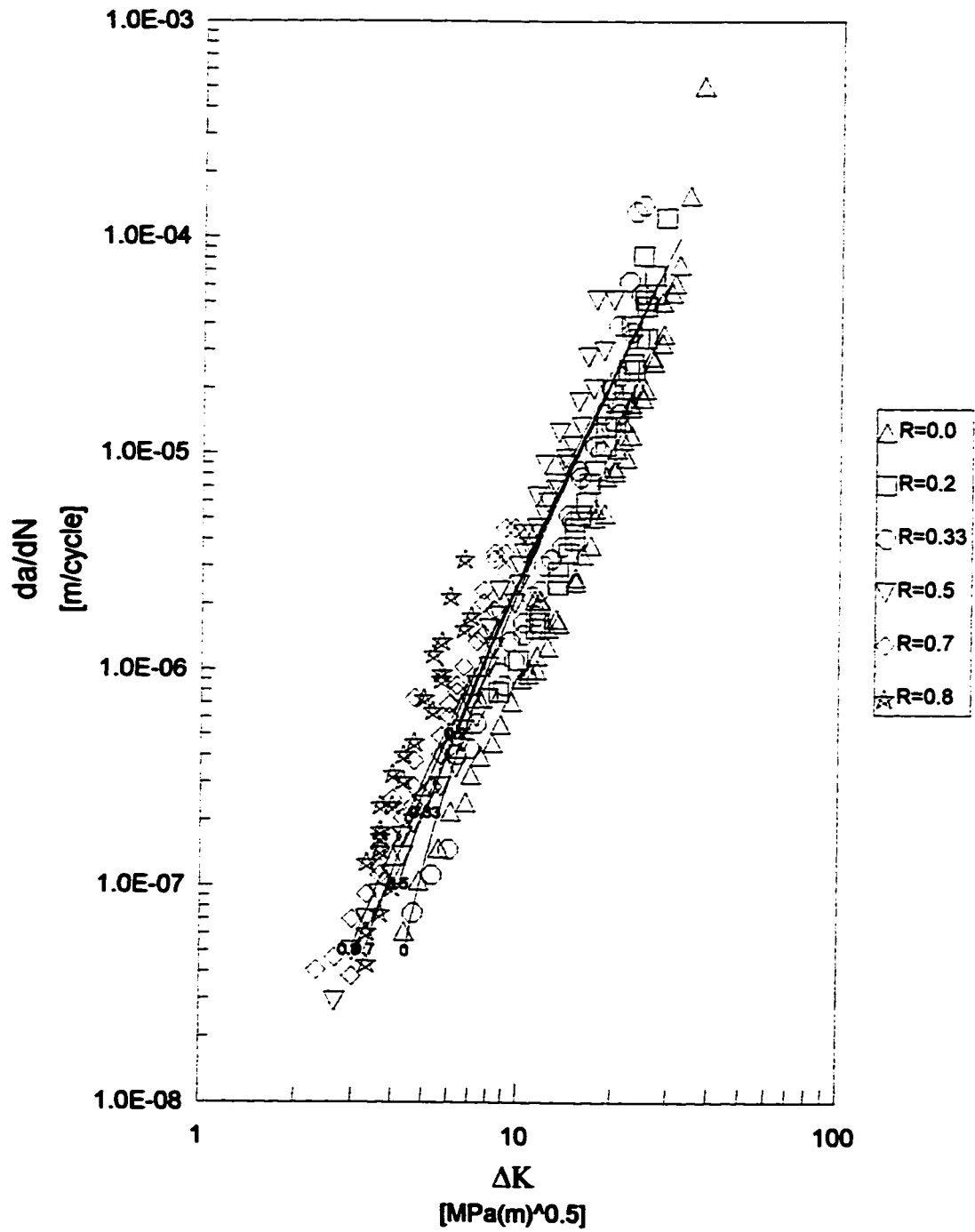


Figure 22 - Correlation of the Proposed Model with the Experimental Data for Aluminum 2024-T3

